2017

Developing protocols for analysis of cellular adaptations to peripheral injury in proprioceptive circuits

Garrett Reid Schmidt-McCormack
Iowa State University

Developing protocols for analysis of cellular adaptations to peripheral injury in proprioceptive circuits

by

Garrett Reid Schmidt-McCormack

A thesis submitted to the graduate faculty

in partial fulfillment of the requirements for the degree of

MASTER OF SCIENCE

Major: Neuroscience

Program of Study Committee:
Nicholas D. Jeffery, Co-major Professor
Jeffrey Trimarchi, Co-major Professor
Mark Ackermann

Iowa State University

Ames, Iowa

2017

I would like to dedicate this thesis to my family for supporting me and nurturing my interest in biological sciences. I would in particular like to dedicate this to my wife, Jennifer Schmidt-McCormack, who has loved and supported me throughout my graduate education.

TABLE OF CONTENTS

LIST OF FIGURES

Chapter 2

Chapter 3

ACKNOWLEGEMENTS

I would like to thank the members of my lab, my adviser Dr. Nicholas Jeffery, Drs. Hilary Hu and Sina Safayi, and Pongrat Jaisil, who all have helped me in various ways. I would also like to thank the members of Dr. Anumantha Kanthasamy's lab for providing me with workspace in their lab and for teaching me patiently how to use the equipment, in particular Matthew Neal, Monica Langley, Shivani Ghaisas, and Dan Luo. Thanks to Kristina Feye for reviewing my thesis and providing moral support. Thanks also to the lab of James Roth for providing us space to perform tissue dissociations.

My co-major professor, Dr. Jeff Trimarchi, and his students, Lauren Laboissonniere and Dr. Jillian Goetz, were of indispensable help. Dr. Trimarchi helped me navigate my way through graduate school. Dr. Goetz first taught me how to perform tissue dissociation. Lauren corresponded with me to clarify which kits and tools were available for RNA extraction from single cells.

I would last like to acknowledge the support of my family. My parents encouraged me and supported my undergraduate studies. My grandparents from my earliest years fostered in me an interest in biology. Thanks to my cousin David for being a moral support throughout my time in graduate school. And most importantly, thank you to my patient and understanding wife, Jennifer Schmidt-McCormack, who has been with me for six years, and who has spent most of that time working on her own graduate degree while supporting me through mine.

ABSTRACT

Proprioception, the sense of position and movement of parts of the body is crucial for proper motor control, and its disruption is associated with various pathologies, particularly joint or muscle injury. While there have been studies into the functional changes of proprioception after injury, the underlying cellular and molecular mechanisms underlying this phenomenon are mostly unknown. Pain hypersensitivity following tissue or nerve damage is a possible analog to proprioceptive disruption. Inflammatory and damage-induced pain have been linked to activation of specific signaling pathways as well as the upregulation of various proteins. We set out to elucidate any parallel between injury-associated pain and proprioceptive disruption at the level of the spinal cord and dorsal root ganglia (DRGs). First, we analyzed global gene expression in dorsal root ganglia (DRGs) in a rat model of anterior cruciate ligament (ACL) injury, a condition commonly associated with altered proprioception. Subsequently, we sought to develop a protocol for targeting specific cells in the muscle proprioceptive circuitry, including DRG neurons and gamma motoneurons (γ-MNs) by combining DiI retrograde axonal tracing with single-cell RNA isolation. Preliminary results suggest an upregulation of matrix metalloproteinase 9 (MMP-9) and neurotrophin-4 (NTF-4) in DRG innervating lesioned knees in rats, suggesting neuropathic pain development, but no significant changes were found in any genes specific to proprioceptive afferents. DiI traced to the correct DRG and spinal cord regions, and a dissociated cell produced an adequate quantity of cDNA. The muscle tracing protocol provides a useful tool for further investigating proprioceptive alterations, the potential to modify the protocol for knee injections may further our understanding of complications in recovery from ACL injuries.

CHAPTER 1

INTRODUCTION AND LITERATURE REVIEW

Introduction

Proprioception is frequently disrupted after severe joint injury, and often leads to a decreased quality of life. A major example of this is the sensory deficit in anterior cruciate ligament (ACL) deficient knees. Few studies have examined the underlying cellular mechanisms of this phenomenon, however. Comparatively, much has been discovered regarding the cellular responses of nociceptors to inflammation and nerve damage and how those events lead to neuropathic pain. It is possible that analogous mechanisms are at work in proprioception. To address this, it is important to specifically target proprioceptive sensory neurons and γ-motoneurons (γ-MNs) and analyze their phenotypes after injury. The best approach is likely an animal model using retrograde tracing dyes followed by enzymatic dissociation of the neural tissue in question.

Background

Proprioception, the sense of position and motion of the parts of the body, is one of the main sensory modalities of the body and is indispensable for regulation of motion, balance, and posture. Several medical conditions have been demonstrated to be associated with proprioceptive disruptions including osteoarthritis[1], spinal cord degeneration[2], and joint injury[3–7]. Proprioceptive neurons, like most mechanoreceptive neurons, have large-diameter, myelinated axons, with cell bodies in the dorsal root ganglia (DRG)[8]. At the distal terminals, these cells tend to innervate Golgi tendon organs (GTOs) in tendons and ligaments, and muscle spindles in muscle tissue[9–11]. These are known as A-α or type I afferents (Ia for muscle

spindles[10,11], and Ib for GTOs[9]). Muscle spindles are modulated by specialized motoneurons in the spinal cord. Whereas α-motoneurons (α-MNs) innervate skeletal muscle fibers that contract the muscle, γ-motoneurons (γ-MNs) innervate fibers within the capsule of the muscle spindle[12,13]. These fibers contract, but do not contribute to overall muscle contraction, and instead put more tension on the muscle spindle, making it functionally more sensitive to stretching.

Proprioception has been studied in terms of muscle electrophysiology[6,14–19] and physical function[3,5,6,18,20]. However, compared to other sensory modalities, such as pain, proprioception has received little attention from cellular and molecular researchers. In this review and the following papers, I will discuss the importance of proprioception in motor function, the disruption of proprioception in anterior cruciate ligament (ACL) injured knees, similar changes in pain models, and potential techniques for further studying these affects.

Proprioception and Function

Effective locomotor function relies on proprioceptive circuitry. Information from proprioceptive fibers is typically necessary to initiate voluntary movement[21], and lack of such inputs subsequent to injuries, such as dorsal column spinal lesion[2], often results in ataxia. Perhaps the primary means by which proprioceptive afferents modulate limb and body movement is by mediating the stretch reflex. Sudden stretches of a muscle cause excitation of muscle spindle fibers, which project to the ventral horn of the spinal cord and excite motor neurons of the same muscle, causing it to contract and resist the motion[22]. In addition to eliciting a stretch response in the stimulated muscle, proprioceptors can also act synergistically with circuits of associated muscles. The Ia afferent neurons from muscle spindles, for example,

synapse with inhibitory interneurons that innervate motoneurons of opposing muscles. This way, the muscle opposing the contracted muscle relaxes, preventing co-contraction.

A further synergistic function of proprioception is the influence of ligament and tendon afferents on muscle afferent sensitivity. One study found that in deeply anesthetized cats, applying a 40 N stretch to the posterior cruciate ligament of the knee increased the firing rate of soleus and semitendinosus muscle sensory fibers during sinusoidal stretching[23]. Since this effect could be canceled by cutting the posterior articular nerve of the knee joint, the researchers determined the effect was due to stimulation of γ-MNs of the muscles in question. Therefore, it is evident that muscle proprioceptive systems are reliant on proprioceptive information from ligaments and tendons to acclimate sensitivity. A later study in dogs demonstrated a similar link between the cranial cruciate ligament (CCL) and the hamstring muscles[17].

Distinct sensory neurons of the DRG are responsible for proprioceptive input. Evidence for this can be seen in genetically modified animal models lacking primary proprioceptive inputs, which suffer sensory ataxia, as pioneered by Ernfors and colleagues in 1994[24]. A knockout mouse line was created by effectively deleting the gene encoding Neurotrophin 3 (NT3) which is crucial for the survival of both mechanically-sensitive primary sensory neurons and motor neurons in the spinal cord. The $NT3^{-/-}$ mice experienced difficulty in placing limbs for movement, occasionally going rigid in all limbs. Upon necropsy $NT3^{-/-}$ mice lacked proprioceptive DRG neurons as well as Ia fibers compared to wild-type controls. More recently, a study showed that targeted knockout of proprioceptive afferents resulted in adult mice exhibiting motor deficits due to mistimed muscle contractions in comparison to control

animals[14]. The researchers noted this was due to the breakdown of patterns typically observed in walking and swimming.

Conversely, an overabundance of proprioceptive input can be detrimental to proper motor function as well. Transgenic mice that overexpress NT3 in skeletal muscles develop excess numbers of large diameter sensory axons and large diameter cells in DRG[25]. This resulted in significantly widened steps compared to wild-type littermates, and to severely decreased performance on balance beam and rotarod tests. Taken all together, the evidence suggests that homeostasis of NT3 signaling and, more importantly, fine-tuned proprioceptive faculties are necessary for motor control.

Disruption of Proprioception and the ACL Model

Proprioception can be disrupted as a result of aging[26,27] or injury[3–7,15,18,20]. Elderly human subjects tend to exhibit weaker electromyographic (EMG) responses in response to electrical stimulation of the sensory nerve (H-reflex) than younger individuals. This is particularly crucial to motor and posture control in the case of soleus muscle H-reflex[26,27]. Younger subjects have selectively diminished H-reflexes in the soleus muscle while standing than while lying prone, preventing a reflexive contraction from disrupting their balance. In older subjects, the soleus H-reflex is weak when tested in either position.

Joint injuries and inflammation are common causes of proprioceptive dysfunctions, with one of the most common locations being the knee joint. Among the most common knee injuries is rupture of the ACL. Human athletes are at high risk of injury, and many patients do not sufficiently regain previous levels of activity afterward[18]. Structural stability can reliably be regained in ACL after rupture through surgical reconstruction using a graft from another tendon

on the patient's leg (autograft) or from using donor tissue (allograft). This stability is typically measured in terms of laxity, or the distance the tibia will shift forward in response to applied pressure. This is expressed as a differential between the laxity of the injured knee and that of the uninjured knee, using an arthrometer[5,6]. There are also measures for activity and function of the knee joint in patients after ACL injury. Two common assessments are the Lysholm and Tegner scales, which score the knee joint based on a questionnaire about a patient's level of activity and quality of life[28]. A common problem for patients unable to return to previous levels of activity is the sensation that the knee is going to "give way," or that there is a sensation of knee failure when sub-failure stress is applied to an otherwise stable knee[6,29].

Controversy remains as to whether reconstructive surgery or conservative treatment and rehabilitation are the best course of action[5,30,31], with some studies suggesting that surgery increases the risk of osteoarthritis later[30]. Conversely, several studies have shown better function of the knee in patients who undergo reconstructive surgery after ACL rupture[5,31]. In a study using matched pairs, patients who underwent reconstruction had better outcomes based on questionnaires regarding activity[31].

Importantly, the ACL appears to have a role in providing more than just a direct mechanical support to the knee joint. It serves as a sensory organ for detecting motion and position of the knee[5], and for mediating stabilizing muscle responses[16,32–34]. Early evidence for this came from histological studies which found sensory endings[32,35]. In particular, sections on the CCL of a cat revealed structures that were likely Golgi tendon organs (GTO) and others that were potentially Pacinian corpuscles, which respond to stretch and vibration respectively.

The presence of a hamstring reflex in response to ACL stimulation serves as direct functional evidence of its role in proprioception. When pressure is applied to the leg to cause mild anterior translation of the tibia, an EMG response is reliably detected in the hamstring[6,34,16,33,36]. This same phenomenon is also observed in dogs[37]. Recent work has shown in humans that this response follows a predictable pattern, where an initial response is detected at 20 ms after stimulation (short latent response, SLR) and another is detected at around 35 ms (medium latent response, MLR)[6,36]. Intraoperative mechanical stimulation of the ACL has verified its role in this reflex[34]. Therefore, it is reasonable to conclude that proprioceptive information directly from the ACL synapses with motor circuitry to stabilize the knee.

In recovery, a return to previous activities is associated with both self-reported satisfaction with the knee and with proprioceptive function[1]. Beard and colleagues found that knee laxity in un-reconstructed ACL-ruptured patients was not significantly correlated with perceived stability of the knee, measured by the frequency of the "giving-way" sensation[15]. However, knee stability was strongly and significantly correlated to the delay of the hamstring reflex in comparison to the uninjured knee. Further studies in humans and dogs have consistently shown a delayed hamstring reflex MLR in legs with ACL ruptures[6,37].

There is still controversy as to whether proprioceptive fibers reinnervate grafted tissue. When Ochi and colleagues applied mechanical stimulation to reconstructed ACLs intraarticularly, somatosensory evoked potentials were detected via electroencephalogram (EEG)[38]. However, in a model using electrical stimulation, Krogsgaard found that much higher currents were required to stimulate reflex responses in reconstructed ACLs compared to the

intact Posterior cruciate ligament (PCL), and that this was most likely what they term “overflow stimulation” in neighboring PCLs[29]. In biopsies of Achilles tendon grafts, no evidence was found of complete proprioceptive endings, though other newly-developed structures were found[39].

It is unclear how various proprioceptive changes occur in injured knees, or what affects their severity. While the research described above has shown improvements after reconstruction, a neuropathological phenotype remains in some otherwise-healthy individuals. A potential analog to this is in neuropathic pain generated by inflammation or peripheral injury. Nociceptive neurons show increased sensitivity subsequent to various experimental conditions. If similar changes occur in proprioceptors, it could be a mechanism for the “giving-way” sensation.

Chronic Pain Models

Thermal and mechanical hypersensitivity are hallmarks of nerve damage and chronic inflammation. Inflammation and nerve damage have both been shown to induce molecular and functional phenotypic changes in nociceptors. Immunohistochemical analysis has linked nerve ligation and axotomy with upregulation of a distinct set of proteins[40–43]. Similar results have been found in models of skin and muscle inflammation as well as arthritis[44–46]. Three mechanisms are believed to be involved in peripheral nociceptor sensitization: neuroinflammation, alteration of calcium-mediated signaling, and changes in membrane potential.

The links between inflammatory events and sensory changes are well documented. Arthritis has been induced in rodent models by lesioning the CCL, resulting in decreased weight bearing on the injured limb, as well as a lower threshold of heat and mechanical stimulation

required before the paw is withdrawn in comparison to controls[47]. In rats with Complete Freund's Adjuvant (CFA)-induced knee arthritis, animals began to struggle at lesser angles of passive motion on arthritic knees in comparison to the contralateral joint[48]. Carrageenan injected into either the knee or the hamstring produced similar results, although pain behavior was elicited in the contralateral side with higher-dose injections[49]. Following ligation of the fifth lumbar (L5) spinal nerve, paw withdrawal threshold in response to pressure on the skin was decreased to less than 20% of control levels for at least two weeks post operation[40].

Phenotypic changes in injured afferents are possibly a result of mitogen activated protein kinase or extracellular-signal-related kinase (MAPK/ERK)-pathway-mediated neuroinflammation. A greater percentage of lumbar DRG neurons were immunopositive for phosphorylated ERK following CFA injections, and this effect was further increased in tissues collected shortly after passive motion of the knee joint[48]. Both inflammation and spinal nerve ligation result in activation of p38-MAPK[40,44]. Inhibiting p38-MAPK activation was shown to reduce heat hyperalgesia[44] and mechanical allodynia[40]. MAPK pathways are subject to signaling from G-protein coupled receptors (GPCRs), interleukin receptors (ILRs) and growth factor receptors (GFRs)[50]. It is possible that in response to injury, the growth-related function of MAPK cascades is important for recovery in sensory neurons, but that the pro-inflammatory pathways result in a collateral contribution to neuropathological conditions.

In all models of inflammation and nerve injury, Activating Transcription Factor 3 (ATF3) has been detected in the nuclei of all neuronal types[41,42,46,51]. This has previously been established as a reliable marker of neural response to injury, reaching peak expression after five to seven days[52]. ATF3 is a member of the Cyclic-AMP-Response-Element-Binding (CREB) protein

family[53], though in reality it has a repressive effect on the transcription of its target genes. It is typically located in the nucleus and is activated by calcium- and cAMP-dependent kinases that are transported from the cytoplasm. Like the MAPK family, ATF3 has been demonstrated in neurons to be crucial for regeneration after injury[42].

Another group of proteins involved in neuroinflammatory pathway of neuropathic pain is the matrix metalloproteinases (MMPs). Short-term responses to nerve-injury include an upregulation in MMP-9[43,45], followed by a later phase marked by MMP-2 upregulation[45]. MMP-9 may mediate pain via the cleavage and activation of extracellular interleukins[54]. Evidence suggests that ATF3 and MAPK have important regulatory functions on MMP activity after inflammation. ATF3 down-regulates MMP-2 by repressing its transcription[51], and so may be important for ending the inflammatory phase of nerve injury. Conversely, inflammation-induced upregulation of MMP-9 is dependent on MAPK[55]. It is unknown how relevant this is to proprioception. It remains to be seen whether there are any analogues.

Further reduced thresholds of pain sensitivity are most likely due, in part, to electrophysiological changes in affected cells. Axotomized A-fiber neurons traced from plantar muscle and skin exhibited oscillations in response to sub-threshold depolarizations[56]. These oscillations, in turn, resulted in repeated action potentials. Following intraplantar injections of CFA, large-diameter DRG neurons in rats expressed increased peak current and relative conductance[57]. Wu and Henry found that in Aβ-fibers from knees with experimentally-induced arthritis, action potential rise-rate was slower and action potential duration was longer when compared with control fibers[58]. This same effect was not observed in c-fibers. In a later study,

they also found a lower threshold and increased rate of fire from Aβ-fibers of arthritic joints[59]. This suggests an alteration of the ion channels expression in inflamed and damaged axons.

Specific voltage gated sodium channels (Na_v) have been mechanistically tied to decreased pain threshold and increased signalling. Tetrodotoxin (TTX)-resistant sodium channels $Na_v1.8$[57,60] and $Na_v1.9$[61] appear to mediate chronic pain and allodynia. Large sensory neurons in CFA-treated rats had lower thresholds even when treated with TTX[57]. More $Na_v1.8$ immunopositive neurons were found in DRGs from these animals. In another study, treatment with RNA antisense to *scn10a* (the gene for $Na_v1.8$) increased paw withdrawal thresholds, and decreased TTX-resistant currents[60]. In a carrageenan model of hindpaw inflammation, $Na_v1.9$-knockout mice did not show the same level of pain behavior as wild-type animals[61]. This behavior was ameliorated in wild-type subjects when treated with antisense RNA to knock down $Na_v1.9$ expression. Interestingly, inflammation did not result in an upregulation in $Na_v1.9$ mRNA in wild-type mice. Since antisense RNA could still decrease $Na_v1.9$ activity, it suggests that inflammation increases translation due to an underlying epigenetic mechanism. A possible analogous situation to this in proprioceptors is the *de novo* expression of $Na_v1.7$, a TTX-sensitive channel, that has been observed following spinal nerve ligation[62].

The above described evidence gives reason to believe that proprioceptive afferents may be sensitized via a pathway analogous to that of pain fibers following nerve damage or inflammation of sensory target tissue. As mentioned, certain proteins are upregulated in all DRG neurons following injury. It is also worthy of note that much of the pain activity was mediated by large, mechanically-activated neurons, which share certain features with proprioceptors, such as the neurotrophin receptor TrkC [8,63]. It is yet to be determined whether

proprioceptive fibers do undergo changes analogous to those of nociceptors in response to injury. If so, a further question is how the different modalities, proteins, and central terminals proprioceptors affect these phenomena in comparison to those of nociceptors, and how the consequences of these pathways differ.

Experimental Approaches for Targeted Proprioceptor Analysis

Past research on proprioceptive deficits specific to joint injury have focused mainly on clinical models looking at EMG and overall sensory function. Conversely, experiments looking at the effects of damage to the target tissue have nearly all been done in view of pain models. Full understanding of proprioceptive changes requires analysis of cellular and molecular responses as well. In one injury model, proprioceptive neurons expressed ATF3 after sciatic nerve axotomy or spinal nerve ligation[41]. In a nerve-crush model of injury, Taylor and colleagues found that mice overexpressing NT3 recovered proprioceptive function sooner than wild-type mice[25]. However, these mice also had proprioceptive deficits before the injury.

There is a need for proprioceptive animal models with no congenital deficit before injury, and in which the molecular phenotype of cells directly involved can be isolated. One of the greatest challenges is isolating the individual neurons innervating a given target and separating them from surrounding cells. To this end, we suggest the combined use of retrograde tracers with enzymatic tissue dissociation, allowing the collection of single cells for gene-expression analysis. Such combinations have already been used successfully for electrophysiological studies[56,61,64]. Further steps can then be taken to cull non-proprioceptive DRG neurons and α-MNs.

Retrograde axonal tracing dyes

Many compounds are available for tracing the axons of cells from target tissue. The two major groups are viral and chemical tracers[65,66]. Tracers for proprioceptive experiments must be long-lasting, readily taken up by nerve terminals, and must not have a severe impact on the function of the target cells. Many traditional tracing methods have drawbacks that are not compatible with these requirements.

Viral tracers typically use rabies[66,67] or herpes[68] virus. They are reliable tracers but are problematic because they, by necessity, must alter the physiology of the cell. Viruses alter gene expression in order to replicate. In addition to being a potential confounding variable, this often leads to the degeneration and death of the traced cells[69]. The destruction of the cells you wish to analyze means that viral tracers are limited to use in studies on connectivity and neuroanatomy.

Chemical tracers mainly include enzymes, bacterial toxins, and fluorescent dyes. Two of the more frequently used tracers for histological studies are horseradish peroxidase[70] (HRP) and cholera toxin B (CTB)[66]. HRP and CTB both require extensive histological processing, and have short detection times within living tissue[65]. This makes them less suited for experiments involving long-term response of sensory and motoneurons to peripheral events.

Fluorescent dyes are ideal for identifying neurons in extended experiments for several reasons: most have not been shown to by cytotoxic, they require no immunological or enzymatic treatment to visualize, and they are detectable for weeks or months after treatment[65]. Three of the most popular dyes for such studies are FastBlue, FluoroGold, and DiI.

One of the popular and effective retrograde tracing dyes is Fast Blue (FB). It is water soluble and resistant to photobleaching[71]. Injected intramuscularly (IM), it traces both sensory and motor fibers[72,73]. In a severed-nerve model, it was shown to label the maximum number of motoneurons at 12 weeks, and persist until at least 24 weeks[71]. It is actively transported through the axon, and may reach the soma in 5 days from most injection sites.

Fluoro-Gold (FG) is a water-soluble fluorescent dye commonly used in retrograde tracing of neurons. At physiological pH, it typically appears green-yellow when viewed under UV fluorescence with no filters in the visible spectrum. FG is typically administered dissolved in 0.9% saline[74], and is readily taken up by sensory terminals, and can trace most fibers in a rat's body within a week[71,75,76]. It has been used in numerous studies for tracing the knee joint in animal models by injecting a solution into the joint capsule[48,77,78]. Unfortunately, FG is only suitable for short-term experiments of less than three weeks, since the number of positive cells begins to decrease after four weeks and one week is required for tracing[71,75]. Additionally, FG is more susceptible to photobleaching in aqueous solutions[76], making it more challenging to use for picking cells.

The lipophilic molecule DiI has long carbon sidechains that allow it to become integrated into the membrane. This allows for passive transport of DiI by diffusion along the membrane, and allows for the tracing of fixed tissues in dead animals[79]. However, this same feature of DiI means it is slower to reach the cell bodies than other fluorescent dyes. DiI has been shown capable of tracing axons innervating various types of tissue, including joint[75], muscle[80], and skin[81]. IM injections of DiI have been used to identify both sensory neurons and motoneurons[80].

It is well-suited for long-term studies as it can be detected as much as nine months after treatment[75].

The lipophilic nature of DiI creates two problems, however. The first problem is that diffusion traces much more slowly than the active transport that carries other fluorescent dyes. Fortunately, this does not make it incompatible with long-term studies on proprioceptors. The second problem is that DiI does not readily dissolve in water or saline. This can be an obstacle in delivering the dye to the target tissue. To address the latter problem DiI can be suspended in these solutions by first dissolving thoroughly in dimethylsulfoxide (DMSO)[82,83]. Unfortunately, DMSO can be cardiotoxic when chronically administered to mice at high doses intraperitoneally[84], and small doses of intraocular DMSO were shown to induce apoptosis in retinal ganglion cells[85]. This toxicity in other tissues has not been observed at small doses in muscle or joint tissue, which is why it has frequently been used for IM injections of fluorescent tracers in mice, typically at around 10% in solution[83,86].

Techniques for single-cell isolation

The appropriate tissue dissociation technique is important for obtaining intact cells with high-quality RNA and without confounding material. This typically involves placing the tissue into a buffered solution of proteolytic enzymes. The particular enzymes and their concentration required will depend on the animal and on the tissue, as the matrix protein makeup can differ based on these factors.

One of the most commonly used proteases is trypsin. Trypsin is an effective serine protease derived from pancreatic tissue. It is one of the more quickly-acting enzymes available for tissue dissociation, and is favored in many cell culture techniques. Some researchers,

however, have found it to be too cellulolytic and have stated a preference not to use it[87]. This presents a challenge when looking at the small populations of target-delineated cells. However, some electrophysiologists have successfully used it and obtained traced cells for patch clamping[56]. Furthermore, other researchers have used alternative enzymes with satisfactory results, even for single-cell gene expression profiling[88,89].

Other commonly used enzymes for neural tissue are collagenase and papain. Collagenase hydrolyzes the bond between the glycine residue connected to its backbone nitrogen. This is a much gentler process than trypsin, and is often used in conjunction with dispase[87,90]. Papain is derived from papaya latex and cleaves the bond at the carboxyl end of an arginine or lysine following a hydrophobic residue. It is typically used in less physically robust tissues, such as the retina[91]. A few protocols have used papain following collagenase for dissociating DRGs[87,90]. However, papain is typically activated using ethylenediamenetetraacetic acid (EDTA), an inhibitor of collagenase activity. It remains to be tested whether following papain with collagenase provides a greater number of intact cells than collagenase alone, as the latter option is a possibility[92], and changing out enzyme solutions could result in a loss of cells.

Cell-type specification

While changes may be expected in nociceptors in response to target-tissue damage (and α-MNs in the case of muscle traces), these are likely to involve different genes and would likely skew or confound the results of an experiment. It is therefore necessary to identify the correct and incorrect cell populations, and either separate them before harvesting RNA, or separate them based on gene expression profile.

Identifying proprioceptors among DRG neurons and γ-MNs in the spinal cord can both be done to some extent based on size. Proprioceptive DRG neurons tend to be of larger diameter than most nociceptors[8,63]. However, there is no guarantee that all cells within the targeted size range will be proprioceptors, as there is significant overlap with non-proprioceptive mechanoreceptors. Size differentiation is more reliable in spinal motoneurons, as motoneurons with a cross-sectional area below 300 μm^2 are almost entirely γ-MNs, while those above 500 μm^2 are nearly all α-MNs[72,93]. Again, this is still not entirely reliable, as there is some size overlap beyond these points, and γ-MNs over the size threshold would be lost, which is problematic when the cell population of interest is already small.

A more reliable way to determine cell type is to use a cell-specific gene as a marker. In the DRG, proprioceptors persistently express parvalbumin, whereas other neurons do not express it at all[94]. In the ventral horn of the spinal cord, γ- and α-MNs can be distinguished from their expression of Err3 and NeuN respectively[72,93]. These markers can be taken advantage of in two ways. The first is to acquire or construct a transgenic line where cells expressing the marker also express a fluorescent protein (that doesn't overlap with the fluorescence profile of the tracer dye). This would allow for selecting cells of the correct type before they are collected for RNA extraction. The second way to utilize these markers is to sort out the data after gene expression profiles have been made. If multiplexed single-cell quantitative polymerase chain reaction (qPCR) is used, testing for marker-gene expression can be used as a criterion for inclusion. Similarly, if RNA-Seq is used, cell profiles can be sorted into various discrete cell types[95,96].

Conclusions

Proprioceptive deficits following joint injury models have been well-documented and tested in clinical patients and animals, but the underlying cellular mechanisms have been left relatively unexamined. Pain models in primary nociceptive pathways under nerve injury and inflammation models have been extensively studied, and point to a role of neuroinflammation-mediated upregulation of ion channels which in turn decrease the threshold of DRG neurons and an increased sensitivity and rate of action potentials. Many of the upstream signaling proteins involved in these phenomena are also upregulated in proprioceptive neurons in the same models. This then begs the question of whether disrupted proprioception, including the feeling of “giving way” in otherwise stable knees, is mediated by analogous pathways. Perhaps proprioceptive deficiencies are comparable in molecular pathway to peripheral neuropathic pain.

References

1. Barrett, D. S., Cobb, A. G. & Bentley, G. Joint proprioception in normal, osteoarthritic and replaced knees. *J. Bone Joint Surg. Br.* **73,** 53–56 (1991).
2. Hankey, G. J. & Edis, R. H. The utility of testing tactile perception of direction of scratch as a sensitive clinical sign of posterior column dysfunction in spinal cord disorders. *J. Neurol. Neurosurg. Psychiatry* **52,** 395–398 (1989).
3. Tyler, T. F., McHugh, M. P., Gleim, G. W. & Nicholas, S. J. Association of KT-1000 measurements with clinical tests of knee stability 1 year following anterior cruciate ligament reconstruction. *J. Orthop. Sports Phys. Ther.* **29,** 540–545 (1999).
4. Jerosch, J., Prymka, M. & Castro, W. H. M. Proprioception of the knee joints with a lesion of the medial meniscus. *Acta Orthop. Belg.* **62,** 41–45 (1996).
5. Reider, B. *et al.* Proprioception of the knee before and after anterior cruciate ligament reconstruction. *Arthroscopy* **19,** 2–12 (2003).
6. Melnyk, M., Faist, M., Gothner, M., Claes, L. & Friemert, B. Changes in stretch reflex excitability are related to 'giving way' symptoms in patients with anterior cruciate ligament rupture. *J. Neurophysiol.* **97,** 474–480 (2007).
7. Katayama, M. *et al.* Proprioception and performance after anterior cruciate ligament rupture. *Int. Orthop.* **28,** 278–281 (2004).
8. Chen, C., Zhou, X. F. & Rush, R. A. Neurotrophin-3 and trkC-immunoreactive neurons in rat dorsal root ganglia correlate by distribution and morphology. *Neurochem.Res.* **21,** 809–814 (1996).
9. Fukami, Y. Responses of isolated Golgi tendon organs of the cat to muscle contraction

and electrical stimulation. *J. Physiol.* **318,** 429–443 (1981).

10. Hunt, C. C. The effect of stretch receptors from muscle on the discharge of motorneurons. *J. Physiol.* **117,** 359–79 (1952).

11. Eccles, R. M. & Lundberg, A. Integrative pattern of Ia synaptic actions on motoneurones of hip and knee muscles. *J. Physiol.* **144,** 271–298 (1958).

12. Bessou, P., Emonet-Denand, F. & Laporte, Y. Motor fibres innervating extrafusal and intrafusal muscle fibres in the cat. *J. Physiol.* **180,** 649–672 (1965).

13. Kuffler, S. W., Hunt, C. C. & Quilliam, J. P. Function of medullated small-nerve fibers in mammalian ventral roots; efferent muscle spindle innervation. *J. Neurophysiol.* **14,** 29–54 (1951).

14. Akay, T., Tourtellotte, W. G., Arber, S. & Jessell, T. M. Degradation of mouse locomotor pattern in the absence of proprioceptive sensory feedback. *Proc. Natl. Acad. Sci. U. S. A.* **111,** 16877–82 (2014).

15. Beard, D. J., Kyberd, P. J., Fergusson, C. M. & Dodd, C. a. Proprioception after rupture of the anterior cruciate ligament. An objective indication of the need for surgery? *J. Bone Joint Surg. Br.* **75,** 311–315 (1993).

16. Dyhre-Poulsen, P. & Krogsgaard, M. R. Muscular reflexes elicited by electrical stimulation of the anterior cruciate ligament in humans. *J. Appl. Physiol.* **89,** 2191–2195 (2000).

17. Miyatsu, M. *et al.* The physiology of mechanoreceptors in the anterior cruciate ligament. *J. Bone Jt. Surg.* **75B,** 653–657 (1993).

18. Courtney, C., Rine, R. M. & Kroll, P. Central somatosensory changes and altered muscle synergies in subjects with anterior cruciate ligament deficiency. *Gait Posture* **22,** 69–74

(2005).

19. Bryant, A. L., Creaby, M. W., Newton, R. U. & Steele, J. R. Hamstring antagonist torque generated in vivo following ACL rupture and ACL reconstruction. *Knee* **17,** 287–290 (2010).

20. Barrett, D. S. Proprioception and function after anterior cruciate reconstruction. *J. Bone Jt. Surg.* **73,** 833–837 (1991).

21. Prochazka, A. Proprioception during voluntary movement. *Can. J. Physiol. Pharmacol.* **64,** 499–504 (1986).

22. Cohen, L. A. Localization of stretch reflex. *J. Neurophysiol.* **16,** 272–285 (1953).

23. Sojka, P., Johansson, H., Sjölander, P., Lorentzon, R. & Djupsjöbacka, M. Fusimotor neurones can be reflexy influenced by activity in receptor afferents from the posterior cruciate ligament. *Brain Res.* **483,** 177–183 (1989).

24. Ernfors, P., Lee, K.-F., Kucera, J. & Jaenisch, R. Lack of neurotrophin-3 leads to deficiencies in the peripheral nervous system and loss of limb proprioceptive afferents. *Cell* **77,** 503–512 (1994).

25. Taylor, M. D. *et al.* Postnatal regulation of limb proprioception by muscle-derived neurotrophin-3. *J. Comp. Neurol.* **432,** 244–258 (2001).

26. Angulo-Kinzler, R. M., Mynark, R. G. & Koceja, D. M. Soleus H-reflex gain in elderly and young adults: modulation due to body position. *J. Gerontol. Med. Sci.* **53,** M120–M125 (1998).

27. Capaday, C. & Stein, R. B. Amplitude modulation of the soleus H-reflex in the human during walking and standing. *J. Neurosci.* **6,** 1308–1313 (1986).

28. Tegner, Y. & Lysholm, J. Rating systems in the evaluation of knee ligament injuries. *Curr. Orthop. Pract.* **198,** 42–49 (1985).

29. Krogsgaard, M. R., Fischer-Rasmussen, T. & Dyhre-Poulsen, P. Absence of sensory function in the reconstructed anterior cruciate ligament. *J. Electromyogr. Kinesiol.* **21,** 82–86 (2011).

30. Kessler, M. a. *et al.* Function, osteoarthritis and activity after ACL-rupture: 11 Years follow-up results of conservative versus reconstructive treatment. *Knee Surgery, Sport. Traumatol. Arthrosc.* **16,** 442–448 (2008).

31. Wittenberg, R. H., Oxfort, H. U. & Plafki, C. A comparison of conservative and delayed surgical treatment of anterior cruciate ligament ruptures. *Int. Orthop.* **22,** 145–148 (1998).

32. Sjölander, P., Johansson, H., Sojka, P. & Rehnholm, a. Sensory nerve endings in the cat cruciate ligaments: a morphological investigation. *Neurosci. Lett.* **102,** 33–38 (1989).

33. Tsuda, E., Okamura, Y., Otsuka, H., Komatsu, T. & Tokuya, S. Direct evidence of the anterior cruciate ligament-hamstring reflex arc in humans. *Am. J. Sports Med.* **29,** 83–87 (2001).

34. Friemert, B. *et al.* Intraoperative direct mechanical stimulation of the anterior cruciate ligament elicits short- and medium-latency hamstring reflexes. *J. Neurophysiol.* **94,** 3996–4001 (2005).

35. Freeman, M. a & Wyke, B. The innervation of the knee joint. An anatomical and histological study in the cat. *J. Anat.* **101,** 505–532 (1967).

36. Schoene, M. *et al.* The reliability of a method for measuring the anterior cruciate

ligament-hamstring reflex: An objective assessment of functional knee instability. *Knee Surgery, Sport. Traumatol. Arthrosc.* **17,** 1107–1116 (2009).

37. Hayes, G. M., Granger, N., Langley-Hobbs, S. J. & Jeffery, N. D. Abnormal reflex activation of hamstring muscles in dogs with cranial cruciate ligament rupture. *Vet. J.* **196,** 345–350 (2013).

38. Ochi, M., Iwasa, J., Uchio, Y., Adachi, N. & Kawasaki, K. Induction of somatosensory evoked potentials by mechanical stimulation in reconstructed anterior cruciate ligaments. *J. Bone Joint Surg. Br.* **84,** 761–766 (2002).

39. Shimizu, T. *et al.* Regeneration process of mechanoreceptors in the reconstructed anterior cruciate ligament. *Arch. Orthop. Trauma Surg.* **119,** 405–409 (1999).

40. Jin, S.-X., Zhuang, Z.-Y., Woolf, C. J. & Ji, R.-R. p38 Mitogen-Activated Protein Kinase Is Activated After a Spinal Nerve Ligation in Spinal Cord Microglia and Dorsal Root Ganglion Neurons and Contributes To the Generation of Neuropathic Pain. *J. Neurosci.* **23,** 4017–4022 (2003).

41. Shortland, P. J. *et al.* ATF3 expression in L4 dorsal root ganglion neurons after L5 spinal nerve transection. *Eur. J. Neurosci.* **23,** 365–373 (2006).

42. Seijffers, R., Mills, C. D. & Woolf, C. J. ATF3 increases the intrinsic growth state of DRG neurons to enhance peripheral nerve regeneration. *J. Neurosci.* **27,** 7911–7920 (2007).

43. Chattapadhyay, S., Myers, R. R., Janes, J. & Shubayev, V. Cytokine regulatino of MMP-9 in peripheral glia: implications for pathological processes and pain in injured nerve. *Brain. Behav. Immun.* **21,** 561–568 (2007).

44. Ji, R. R., Samad, T. A., Jin, S. X., Schmoll, R. & Woolf, C. J. p38 MAPK activation by NGF in

primary sensory neurons after inflammation increases TRPV1 levels and maintains heat hyperalgesia. *Neuron* **36,** 57–68 (2002).

45. Nascimento, G. C., Rizzi, E. & Gerlach, R. F. Expression of MMP-2 and MMP-9 in the rat trigeminal ganglion during the development of temporomandibular joint inflammation. *Braz. J. Med. Biol. Res.* **46,** 956–967 (2013).

46. Nascimento, D. S. M., Castro-Lopes, J. M. & Neto, F. L. M. Satellite glial cells surrounding primary afferent neurons are activated and proliferate during monoarthritis in rats: Is there a role for ATF3? *PLoS One* **9,** (2014).

47. Hamilton, C. B. *et al.* Weight-bearing asymmetry and vertical activity differences in a rat model of post-traumatic knee osteoarthritis. *Osteoarthr. Cartil.* **23,** 1178–1185 (2015).

48. Seino, D. *et al.* The role of ERK signaling and the P2X receptor on mechanical pain evoked by movement of inflamed knee joint. *Pain* **123,** 193–203 (2006).

49. Radhakrishnan, R., Moore, S. A. & Sluka, K. A. Unilateral carrageenan injection into muscle or joint induces chronic bilateral hyperalgesia in rats. *Pain* **104,** 567–577 (2003).

50. Avruch, J. MAP kinase pathways: the first twenty years. *Biochim. Biophys. Acta* **1773,** 1150–60 (2007).

51. Yan, C., Wang, H. & Boyd, D. D. ATF3 represses 72-kDa type IV collagenase (MMP-2) expression by antagonizing p53-dependent trans-activation of the collagenase promoter. *J. Biol. Chem.* **277,** 10804–10812 (2002).

52. Tsujino, H. *et al.* Activating transcription factor 3 (ATF3) induction by axotomy in sensory and motoneurons: A novel neuronal marker of nerve injury. *Mol. Cell. Neurosci.* **15,** 170–182 (2000).

53. Chen, B. P., Liang, G., Whelan, J. & Hai, T. ATF3 and ATF3 delta Zip. Transcriptional repression versus activation by alternatively spliced isoforms. *J. Biol. Chem.* **269,** 15819–15826 (1994).

54. Berta, T., Liu, T., Liu, Y.-C., Xu, Z.-Z. & Ji, R.-R. Acute morphine activates satellite glial cells and up-regulates IL-1β in dorsal root ganglia in mice via matrix metalloprotease-9. *Mol. Pain* **8,** 18 (2012).

55. Holvoet, S., Vincent, C., Schmitt, D. & Serres, M. The inhibition of MAPK pathway is correlated with down-regulation of MMP-9 secretion induced by TNF-?? in human keratinocytes. *Exp. Cell Res.* **290,** 108–119 (2003).

56. Liu, C. N., Devor, M., Waxman, S. G. & Kocsis, J. D. Subthreshold oscillations induced by spinal nerve injury in dissociated muscle and cutaneous afferents of mouse DRG. *J Neurophysiol* **87,** 2009–2017 (2002).

57. Belkouch, M. *et al.* Functional up-regulation of Nav1.8 sodium channel in Aβ afferent fibers subjected to chronic peripheral inflammation. *J. Neuroinflammation* **11,** 45 (2014).

58. Wu, Q. & Henry, J. L. Changes in Abeta non-nociceptive primary sensory neurons in a rat model of osteoarthritis pain. *Mol. Pain* **6,** 37 (2010).

59. Wu, Q. & Henry, J. L. Functional changes in muscle afferent neurones in an osteoarthritis model: Implications for impaired proprioceptive performance. *PLoS One* **7,** 1–10 (2012).

60. Joshi, S. K. *et al.* Involvement of the TTX-resistant sodium channel Nav 1.8 in inflammatory and neuropathic, but not post-operative, pain states. *Pain* **123,** 75–82 (2006).

61. Lolignier, S. *et al.* Nav1.9 channel contributes to mechanical and heat pain

hypersensitivity induced by subacute and chronic inflammation. *PLoS One* **6,** 1–11 (2011).

62. Fukuoka, T., Miyoshi, K. & Noguchi, K. De novo expression of Nav1.7 in injured putative proprioceptive afferents: Multiple tetrodotoxin-sensitive sodium channels are retained in the rat dorsal root after spinal nerve ligation. *Neuroscience* **284,** 693–706 (2015).

63. Moqrich, A. *et al.* Expressing TrkC from the TrkA locus causes a subset of dorsal root ganglia neurons to switch fate. *Nat. Neurosci* **7,** 812–818 (2004).

64. Flake, N. M. & Gold, M. S. Inflammation alters sodium currents and excitability of temporomandibular joint afferents. *Neurosci. Lett.* **384,** 294–299 (2005).

65. Lanciego, J. L. & Wouterlood, F. G. A half century of experimental neuroanatomical tracing. *J. Chem. Neuroanat.* **42,** 157–183 (2011).

66. Suzuki, L., Coulon, P., Sabel-Goedknegt, E. H. & Ruigrok, T. J. H. Organization of Cerebral Projections to Identified Cerebellar Zones in the Posterior Cerebellum of the Rat. *J. Neurosci.* **32,** 10854–10869 (2012).

67. Beier, K. T., Saunders, A. B., Oldenburg, I. A., Sabatini, B. L. & Cepko, C. L. Vesicular stomatitis virus with the rabies virus glycoprotein directs retrograde transsynaptic transport among neurons in vivo. *Front. Neural Circuits* **7,** 11 (2013).

68. Huang, J., Lazear, H. M. & Friedman, H. M. Completely assembled virus particles detected by transmission electron microscopy in proximal and mid-axons of neurons infected with herpes simplex virus type 1, herpes simplex virus type 2 and pseudorabies virus. *Virology* **409,** 12–16 (2011).

69. Li, X.-Q., Sarmento, L. & Fu, Z. F. Degeneration of neuronal processes after infection with pathogenic, but not attenuated, rabies viruses. *J. Virol.* **79,** 10063–10068 (2005).

70. Kristensson, K. & Olsson, Y. Uptake and retrograde transport of peroxidase in hypoglossal neurones. *Acta Neuropathol.* **19,** 1–9 (1971).

71. Novikova, L., Novikov, L. & Kellerth, J. O. Persistent neuronal labeling by retrograde fluorescent tracers: A comparison between Fast Blue, Fluoro-Gold and various dextran conjugates. *J. Neurosci. Methods* **74,** 9–15 (1997).

72. Shneider, N. A., Brown, M. N., Smith, C. A., Pickel, J. & Alvarez, F. J. Gamma motor neurons express distinct genetic markers at birth and require muscle spindle-derived GDNF for postnatal survival. *Neural Dev.* **4,** 42 (2009).

73. Misawa, H. *et al.* Osteopontin is an alpha motor neuron marker in the mouse spinal cord. *J. Neurosci. Res.* **90,** 732–742 (2012).

74. Schmued, L. C. & Fallon, J. H. Fluoro-Gold: a new fluorescent retrograde axonal tracer with numerous unique properties. *Brain Res.* **377,** 147–154 (1986).

75. Choi, D., Li, D. & Raisman, G. Fluorescent retrograde neuronal tracers that label the rat facial nucleus: A comparison of Fast Blue, Fluoro-ruby, Fluoro-emerald, Fluoro-Gold and DiI. *J. Neurosci. Methods* **117,** 167–172 (2002).

76. Wessendorf, M. W. Fluro-Gold: composition, and mechanism of uptake. *Brain Res.* **553,** 135–148 (1991).

77. Hanesch, U. & Heppelmann, B. A simple method for a specific retrograde labelling of dorsal root and sympathetic ganglion cells innervating the knee joint of the cat. *J. Neurosci. Methods* **63,** 55–59 (1995).

78. Salo, P. T. & Theriault, E. Number, distribution and neuropeptide content of rat knee joint afferents. *J. Anat.* **190 (Pt 4,** 515–522 (1997).

79. Swift, M. J., Crago, P. E. & Grill, W. M. Applied electric fields accelerate the diffusion rate and increase the diffusion distance of DiI in fixed tissue. *J. Neurosci. Methods* **141,** 155–163 (2005).

80. Gautam, M., Benson, C. J. & Sluka, K. A. Increased response of muscle sensory neurons to decreases in pH after muscle inflammation. *Neuroscience* **257,** 2432–2437 (2005).

81. Rau, K. K. *et al.* Cutaneous tissue damage induces long-lasting nociceptive sensitization and regulation of cellular stress- and nerve injury-associated genes in sensory neurons. *Exp. Neurol.* **283,** 413–427 (2016).

82. Seo, T. B. *et al.* ERK1/2-Mediated Schwann Cell Proliferation in the Regenerating Sciatic Nerve by Treadmill Training. *J. Neurotrauma* **26,** 1733–1744 (2009).

83. Zhu, Y., Dua, S. & Gold, M. S. Inflammation-induced shift in spinal $GABA_A$ signaling is associated with a tyrosine kinase-dependent increase in $GABA_A$ current density in nociceptive afferents. *J. Neurophysiol.* **108,** 2581–93 (2012).

84. Kramer, K. *et al.* Effect of dimethyl sulfoxide (DMSO) on the electrocardiogram (ECG) in freely moving male Balb/c mice. *Gen. Pharmacol.* **26,** 1403–1407 (1995).

85. Galvao, J. *et al.* Unexpected low-dose toxicity of the universal solvent DMSO. *FASEB J.* **28,** 1317–1330 (2014).

86. Lindqvist, N., Vidal-Sanz, M. & Hallböök, F. Single cell RT-PCR analysis of tyrosine kinase receptor expression in adult rat retinal ganglion cells isolated by retinal sandwiching. *Brain Res. Protoc.* **10,** 75–83 (2002).

87. Malin, S. a, Davis, B. M. & Molliver, D. C. Production of dissociated sensory neuron cultures and considerations for their use in studying neuronal function and plasticity.

Nat. Protoc. **2,** 152–160 (2007).

88. Johnson, M. B. *et al.* Single-cell analysis reveals transcriptional heterogeneity of neural progenitors in human cortex. *Nat. Neurosci.* **18,** 637–646 (2015).

89. Taniguchi, K., Tomoharu, K. & Kambara, H. Quantitative analysis of gene expression in a single cell by qPCR. *Nat. Methods* **6,** 503–506 (2009).

90. Bosmans, F., Puopolo, M., Martin-Eauclaire, M.-F., Bean, B. P. & Swartz, K. J. Functional properties and toxin pharmacology of a dorsal root ganglion sodium channel viewed through its voltage sensors. *J. Gen. Physiol.* **138,** 59–72 (2011).

91. Goetz, J. J. & Trimarchi, J. M. Single-cell Profiling of Developing and Mature Retinal Neurons. *J. Vis. Exp.* **0,** 1–7 (2012).

92. Hu, H. *et al.* 2-Aminoethoxydiphenyl Borate Is a Common Activator of TRPV1 ,. *J. Biol. Chem.* **279,** 35741–35748 (2004).

93. Friese, A. *et al.* Gamma and alpha motor neurons distinguished by expression of transcription factor Err3. *Proc. Natl. Acad. Sci. U. S. A.* **106,** 13588–93 (2009).

94. Ringstedt, T., Kucera, J., Lendahl, U., Ernfors, P. & Ibanez, C. F. Limb proprioceptive deficits without neuronal loss in transgenic mice overexpressing neurotrophin-3 in the developing nervous system. *Development* **124,** 2603–2613 (1997).

95. Li, C.-L. *et al.* Somatosensory neuron types identified by high-coverage single-cell RNA-sequencing and functional heterogeneity. *Cell Res.* 1–20 (2015). doi:10.1038/cr.2015.149

96. Usoskin, D. *et al.* Unbiased classification of sensory neuron types by large-scale single-cell RNA sequencing. *Nat. Neurosci.* **18,** 145–153 (2015).

CHAPTER 2

A PILOT STUDY IN THE GENE EXPRESSION OF DORSAL ROOT GANGLIA AFTER CRANIAL CRUCIATE LIGAMENT RUPTURE IN RATS

Abstract

Cruciate ligament (ACL/CCL) ruptures are common orthopedic injuries in both human and veterinary patients, commonly resulting in proprioceptive disruptions. We hypothesize that proprioceptive neurons innervating knee joints with ruptured ligaments undergo phenotypic changes analogous to those observed in nociceptors in models of inflammatory and neuropathic pain. In this pilot study, we compared gene expression profiles of whole dorsal root ganglion (DRG) samples from CCL-lesioned rats to those from sham-operated rats using a qPCR array specific for synaptic plasticity. No gene showed a significant change in expression between groups, however matrix metalloproteinase 9 (MMP-9) and neurotrophin 4 (NTF4) both tended to be expressed more highly in the DRG ipsilateral to operated knees in lesioned rats.

Introduction

Cruciate ligament tears are a common, debilitating, and costly orthopedic injury in both human and veterinary patients. The anterior cruciate ligament (or cranial cruciate ligament in veterinary patients, ACL/CCL) is located inside the knee or stifle joint and resists anterior tibial translation and medial tibial rotation. The overall rate of such injuries is unknown, but in the United States, an estimated 130,000 reconstructive surgeries in human patients were carried out in 2006[1]. The annual cost of care for human patients in the U.S. was estimated to exceed $7 billion in 2013[2], and the annual cost in dogs was over $1 billion in 2003[3].

Treatment options typically involve reconstructive surgery and have promising success rates in restoration of mechanical stability[4,5]. Unfortunately, this does not necessarily result in a full return to function. Patients have frequently reported a feeling of "giving way," or the sensation that the knee is failing, when sub-failure stress is applied to the knee[6,7]. This suggests that the ACL/CCL has an important role in proprioception, and that this function is disrupted after injury.

Supporting the notion of a sensory role for the cruciate ligament is the presence of mechanically-sensitive receptors in histological sections[8,9] and electrical responses to ACL/CCL stimulation observed in hamstring electromyograms (EMG)[6,10–13] giving an initial short latent response (SLR) followed by a medium latent response (MLR). Both human and canine patients demonstrate an altered hamstring reflex EMG after injury. In humans, the MLR of the injured leg is delayed compared to that of the contralateral leg[6]. Dogs also display a delayed MLR after CCL rupture, but it is observed in both the affected and contralateral limb[14]. This suggests that injury of the ACL/CCL has a disruptive effect on proprioception.

Previous research into chronic pain has shown plastic changes in nociceptors after peripheral injury[15–17]. In this pilot study, we aimed to see if phenotypic changes could be observed in terms of gene expression after CCL rupture in a rat model. To this end, we collected RNA samples from whole dorsal root ganglia (DRGs) in rats three weeks after ligament rupture or sham surgery and analyzed them using a quantitative polymerase chain reaction (qPCR) array focusing on synaptic plasticity. No significant changes in gene expression were observed between lesioned rats and controls, but several genes associated with neuropathic pain models were more highly expressed in DRGs ipsilateral to injury. This was followed up with

immunohistochemistry (IHC) of DRG from either side of rats with unilateral CCL lesions, but the data did not support the qPCR results.

Methods

CCL injury model

Twelve adult male Sprague-Dawley rats of 8 to 10 weeks of age were obtained from Charles River Labs and Harlan. Animals were housed two to a cage and all efforts were taken to minimize suffering and discomfort. All procedures were approved by the Iowa State University Institutional Animal Care and Use Committee.

For surgeries, animals were generally anesthetized by 2% isoflurane in oxygen, and kept on a warming pad set on low for the duration. An incision was made on the medial side of the right knee, and the patella was held gently to the side. For eight rats in the experimental condition (four for gene expression, eight for histology), the cruciate ligament was cut using a hooked micro dissection knife (Dean Knife, Roboz). For the other four rats in the sham group, a blunt probe was briefly placed into the knee joint. The surgical sites were then rinsed with sterile saline and sutured closed in layers. Before waking, each rat was given an injection of 0.3 mL (0.009mg) of buprenorphine. Each rat was fed 0.25 mL (0.075 mg) of buprenorphine mixed in Nutella every 12 hours for 48 hours after the operation, and monitored for signs of discomfort.

Tissue collection for gene-expression analysis

Three weeks after operation, animals were deeply anesthetized under 2-5% isoflurane, and given an injection of pentobarbital (Beuthenasia, minimum 0.3 mL per animal) intraperitoneally. This timepoint was chosen to assess the long-term effects of the injury. DRGs

from lumbar 4 and 5 (DRG L4 and 5) were located by following the sciatic nerve up from the leg. DRG L4 and 5 ipsilateral to the operation in each animal were pooled together as one sample, and the DRG L4 and 5 from the contralateral side were taken as a control. After removal, DRG were rinsed in phosphate buffered saline (PBS) and placed in RNA*later* (Ambion) at 4°C overnight. After one night, samples were moved to -20°C.

Reverse transcription quantitative PCR (RT-qPCR)

RNA was extracted using RNeasy Kits (Qiagen) according to manufacturer instructions. Using an RT^2 Nano PreAMP kit (SA Biosciences) 50 ng of RNA from each sample was used to synthesize cDNA which was then pre-amplified. Amplified samples were then analyzed using 96-well RT^2 Profiler Arrays (SA Biosciences) in a StrataGene thermocycler. The contralateral DRG from one of the knee-lesioned rats produced no RNA, and the animal was thus excluded from further analysis.

Tissue collection for immunohistochemistry

DRGs were harvested at 3 weeks and rinsed as before. L4 DRGs were placed in 4% paraformaldehyde (PFA) in PBS at 4° C overnight. The next morning, tissues were transferred to 30% Sucrose at 4° C for 48 hours. Afterward, tissues were embedded in O.C.T. (Tissue Tek) in cryomolds and flash frozen using dry ice. Samples were stored at -80° C until sectioned.

Sections were cut on in a cryostat (Cryostar NX70, Thermo Scientific) with a block and blade temperature of -20° C. 6 µm sections were collected onto Superfrost plus slides (VWR) sequentially across 10 slides in a series at 8 sections per slide. Each sample yielded three series. Slides were dried at around 43° C for 30 minutes before being placed in 5-slide mailers in a

desiccating box overnight. The mailers were sealed using electrical tape and stored at -80° C until further processing.

Immunohistochemistry and image analysis

Slides 1-5 from series 2 on each sample were allowed to acclimate to room temperature for 30 minutes before being unsealed and processed. This series was selected as it was approximately halfway through the DRG for most samples. Sections were washed and stained using a technique previously described[18]. Briefly, cells were washed in three baths of PBS and blocked in 2% BSA with triton X-100 and Tween 20 for 1 hour before being treated overnight with primary antibodies (Rabbit anti-TrkC, Santa Cruz, 1:200; Goat anti-MMP9, Santa Cruz, 1:100) at 4° C. TrkC was selected for analysis, as it is indicative of mechanoreceptive neurons[19,20]. Sections were then washed in more PBS baths, and stained with fluorophore-conjugated secondary antibodies (Affinipure Cy5-conjugated donkey anti-goat, Jackson, 1:100; Affinipure AlexaFluor-488-conjugated donkey anti-rabbit, Jackson, 1:100) for 90 minutes at room temperature. Samples were then washed in PBS, followed by H_2O baths, and finally dried in graded ethanol solutions and HistoClear (Electron Microscopy Sciences). Once dried, sections were mounted with Pro-Long Gold with DAPI (Life Technologies), coverslipped, and cured overnight in a light-proof container. Each set of slides contained a negative control with no primary antibodies.

Immunostained slides were blinded for assessment. Images of slides were obtained using a Nikon inverted microscope (TE-2000U) and a SPOT digital camera (Diagnostic Instruments) and 20X magnification. Using ImageJ, DAPI-stained nuclei were used to select cells

for analysis. DAPI-positive cells were traced by hand, and the mean intensity of fluorescence was measured in both the green and the red channels.

Data analysis

C_T values (the cycle at which the fluorescence threshold is reached) for each gene in a sample were compared against the pooled average of C_T values of four housekeeper control genes in the arrays. A fifth housekeeper encoding β_2 microglobulin (B2M) was excluded, as its C_T value varied widely between samples. The average C_T value of the housekeepers for the plate was subtracted from the C_T of each gene, giving a ΔC_T. For each animal, the ΔC_T values from the sample ipsilateral to operation were subtracted from the ΔC_T value from the contralateral side, generating $\Delta\Delta C_T$ values. For each gene, the average $\Delta\Delta C_T$ values for the CCL-lesioned group were compared to those of the sham-operated group, and a Student's t-test was used to determine the *p*-value. Fold changes between control and operated sides are expressed as $2^{-\Delta\Delta Ct}$. One of the rats from the CCL-lesioned group was excluded from analysis, because the control sample yielded no RNA.

Immunostaining was analyzed in terms of relative expression as previously described[21]. Background fluorescence was determined individually for each section by measuring mean intensity from non-stained nerve tissue and subtracting it from each cells value. This provided the raw mean intensity for each cell. Relative intensity scores were then determined using the formula:

$$Relative\ Intensity\ Score = 100 \times \frac{Raw\ Mean\ Intensity - Minimum\ Intensity}{Maximum\ Intensity - Minimum\ Intensity}$$

Raw Mean Intensity refers to the mean intensity value of the cell being measured, Minimum Intensity is the mean intensity of the DAPI-positive cell at the minimum in that particular slide, and Maximum Intensity is the mean intensity of the DAPI-positive cell with the highest. Data from all rats were pooled, and samples ipsilateral to lesion were compared to those contralateral using a Mann-Whitney *U* test.

Results

Moderate upregulation of Matrix metalloproteinase 9 and Neurotrophin-4 gene expression

Three weeks after injury, DRG were collected from L4 and 5 on both sides of each rat. L4 and 5 from the same side on the same animal were homogenized together, and RNA was extracted, reverse-transcribed, and then analyzed using qPCR arrays. $\Delta\Delta C_T$ was calculated for each gene in each animal by comparing ΔC_T expression between the sides. These values were then pooled for the two groups for between group comparison.

No genes showed significantly different regulation ($p \leq 0.05$). However, there were several points of interest. Matrix metalloproteinase 9 (MMP9) was upregulated in DRGs from the operated side of lesioned animals (Fig 1 heat map, mean $\Delta\Delta C_T$ = -1.41, 2.66-fold increase from contralateral), whereas it was slightly downregulated on average in sham-operated animals (Fig 2 heat map, mean $\Delta\Delta C_T$ = 1.17, 2.25-fold decrease from contralateral). Notably, MMP-9 is associated with increased pain phenotypes in response to inflammation and injury[16,22]. Neurotrophin-4 (NTF4) a neurotrophic factor binding TrkB, was upregulated in the operated side of all lesioned samples (Fig 1, mean $\Delta\Delta C_T$ = -0.72, 1.65-fold increase from contralateral). Expression of NTF4 was lower in the operated side of all sham-operated animals (Fig 2, mean $\Delta\Delta C_T$ = 1.44, 2.71-fold decrease from contralateral).

IHC did not show protein expression supporting qPCR findings

Four rats with surgically lesioned CCLs on the right side were sacrificed three weeks after surgery, and DRG L4 from each side of each animal was collected and prepared for IHC. Sections taken from approximately midway through the DRG were collected onto slides, and immunostained (Fig 3a and 3b) for TrkC (green fluorescence) and MMP-9 (red fluorescence). TrkC expression was assessed in an attempt to discern mechanoreceptive neurons[19]. Relative fluorescence intensity measurements from DRG sections contralateral to injury (Fig 3a) were pooled and compared to the pooled measurements from DRG sections ipsilateral to injury (Fig 3b).

Immunostaining did not support the notion of upregulation of MMP-9 protein in DRG innervating lesioned knees, and in fact contradicted the data from RT-qPCR experiments. Sections from DRGs contralateral to knee lesions showed slightly but significantly higher relative intensity in MMP-9 staining than did ipsilateral sections ($p = 0.0129$, Fig 3c). On the other hand, relative intensity for TrkC immunolabeling was strongly and significantly higher in sections ipsilateral to injury ($p < 0.0001$, Fig 3d). This change in immunoreactivity for TrkC is not expected, and likely indicates some confounding effect since there is no correlation between cell area and relative intensity (Fig 3e) which we would expect there to be[19].

Discussion

Most genes showed no notable change subsequent to either CCL lesion or sham operation, and no changes were statistically significant. Some genes did show a change in expression level, and for some of these genes the lack of significance is due to the small size of the study (n=3 lesioned rats, n=4 sham rats). However, MMP-9 and NTF4 both tended to be

upregulated in DRG innervating lesioned knees. While the results of the IHC experiment contradict the findings of upregulated MMP-9, it should be noted there were some problems with the difference was rather small, and that there were some problems with the slides. First, even though slides did show more fluorescence than negative controls, intensity was week, and long exposure times were required (2022 msec for TrkC, 2960 msec for MMP-9). This is cause to doubt the relevance of the IHC data. Therefore, even though the MMP-9 protein downregulation in DRG ipsilateral to lesion was more significant than the mRNA upregulation, there is more reason to trust the gene expression analysis, and suspect an upregulation of MMP-9 is more likely.

The upregulation of MMP-9 could be important, as it is upregulated in the initial phase (roughly one to three days) after nerve injury or peripheral inflammation[16,22]. It plays a role in mediating further neuroinflammation by cleaving and activating extracellular cytokines[16]. While MMP-9 is only slightly elevated at the three-week timepoint, it is likely that it would show strong upregulation at an earlier timepoint. MMP-9 upregulation peaks at three days post-inflammation, and by day seven it subsides to slightly above control levels[16].

The upregulation of NTF4 could suggest a role in recovery. NTF4 is a member of the neurotrophin family of growth factors, and binds TrkB, the same receptor as brain derived neurotrophic factor (BDNF)[23]. Activation of this receptor is involved in growth and survival of certain subsets of neurons, but in nociceptors, it is also associated with the development of neuropathic pain[24,25]. Less research has been done on NTF4, but it has been tied to activity dependent regeneration of nerve fibers after peripheral damage in a mouse model[26]. A

hypothesis can be drawn, then, that CCL lesion leads to a painful phenotype of afferents that has a gross effect on the DRG.

There is little to be determined in terms of proprioception from this experiment, as none of the genes upregulated are specifically involved in this capacity. Furthermore, cell bodies of proprioceptive fibers innervating the knee make up at most less than 400 cells[27] out of thousands of other neurons in a given DRG, in addition to many more satellite glial cells. Future studies in this direction would benefit from the use of targeted analysis, such as tracing afferents from the joint[27,28]. From this point, cells can be analyzed histologically, or dissociated for single cell transcript profiling[29,30].

References

1. Mall, N. a *et al.* Incidence and trends of anterior cruciate ligament reconstruction in the United States. *Am. J. Sports Med.* **42,** 2363–2370 (2014).
2. Mather III, R. C. *et al.* Societal and Economic Impact of Anterior Cruciate Ligament Tears. *J. Bone Jt. Surgery, Am. Vol.* **95–A,** 1751–1759 (2013).
3. Wilke, V. L., Robinson, D. A., Evans, R. B., Rothschild, M. F. & Conzemius, M. G. Estimate of the annual economic impact of treatment of cranial cruciate ligament injury in dogs in the United States. *J. Am. Vet. Med. Assoc.* **227,** 1604–1607 (2005).
4. Wittenberg, R. H., Oxfort, H. U. & Plafki, C. A comparison of conservative and delayed surgical treatment of anterior cruciate ligament ruptures. *Int. Orthop.* **22,** 145–148 (1998).
5. Reider, B. *et al.* Proprioception of the knee before and after anterior cruciate ligament reconstruction. *Arthroscopy* **19,** 2–12 (2003).
6. Melnyk, M., Faist, M., Gothner, M., Claes, L. & Friemert, B. Changes in stretch reflex excitability are related to 'giving way' symptoms in patients with anterior cruciate ligament rupture. *J. Neurophysiol.* **97,** 474–480 (2007).
7. Krogsgaard, M. R., Fischer-Rasmussen, T. & Dyhre-Poulsen, P. Absence of sensory function in the reconstructed anterior cruciate ligament. *J. Electromyogr. Kinesiol.* **21,** 82–86 (2011).
8. Freeman, M. a & Wyke, B. The innervation of the knee joint. An anatomical and histological study in the cat. *J. Anat.* **101,** 505–532 (1967).
9. Sjölander, P., Johansson, H., Sojka, P. & Rehnholm, a. Sensory nerve endings in the cat

cruciate ligaments: a morphological investigation. *Neurosci. Lett.* **102,** 33–38 (1989).

10. Dyhre-Poulsen, P. & Krogsgaard, M. R. Muscular reflexes elicited by electrical stimulation of the anterior cruciate ligament in humans. *J. Appl. Physiol.* **89,** 2191–2195 (2000).
11. Tsuda, E., Okamura, Y., Otsuka, H., Komatsu, T. & Tokuya, S. Direct evidence of the anterior cruciate ligament-hamstring reflex arc in humans. *Am. J. Sports Med.* **29,** 83–87 (2001).
12. Friemert, B. *et al.* Intraoperative direct mechanical stimulation of the anterior cruciate ligament elicits short- and medium-latency hamstring reflexes. *J. Neurophysiol.* **94,** 3996–4001 (2005).
13. Schoene, M. *et al.* The reliability of a method for measuring the anterior cruciate ligament-hamstring reflex: An objective assessment of functional knee instability. *Knee Surgery, Sport. Traumatol. Arthrosc.* **17,** 1107–1116 (2009).
14. Hayes, G. M., Granger, N., Langley-Hobbs, S. J. & Jeffery, N. D. Abnormal reflex activation of hamstring muscles in dogs with cranial cruciate ligament rupture. *Vet. J.* **196,** 345–350 (2013).
15. Ji, R. R., Samad, T. A., Jin, S. X., Schmoll, R. & Woolf, C. J. p38 MAPK activation by NGF in primary sensory neurons after inflammation increases TRPV1 levels and maintains heat hyperalgesia. *Neuron* **36,** 57–68 (2002).
16. Nascimento, G. C., Rizzi, E. & Gerlach, R. F. Expression of MMP-2 and MMP-9 in the rat trigeminal ganglion during the development of temporomandibular joint inflammation. **46,** 956–967 (2013).
17. Nascimento, D. S. M., Castro-Lopes, J. M. & Neto, F. L. M. Satellite glial cells surrounding

primary afferent neurons are activated and proliferate during monoarthritis in rats: Is there a role for ATF3? *PLoS One* **9,** (2014).

18. Langley, M. *et al.* Mito-apocynin Prevents Mitochondrial Dysfunction, Microglial Activation, Oxidative Damage and Progressive Neurodegeneration in MitoPark Transgenic Mice. *Antioxid. Redox Signal.* **0,** ars.2016.6905 (2017).
19. Chen, C., Zhou, X. F. & Rush, R. A. Neurotrophin-3 and trkC-immunoreactive neurons in rat dorsal root ganglia correlate by distribution and morphology. *Neurochem.Res.* **21,** 809–814 (1996).
20. Moqrich, A. *et al.* Expressing TrkC from the TrkA locus causes a subset of dorsal root ganglia neurons to switch fate. *Nat. Neurosci* **7,** 812–818 (2004).
21. Rau, K. K. *et al.* Cutaneous tissue damage induces long-lasting nociceptive sensitization and regulation of cellular stress- and nerve injury-associated genes in sensory neurons. *Exp. Neurol.* **283,** 413–427 (2016).
22. Holvoet, S., Vincent, C., Schmitt, D. & Serres, M. The inhibition of MAPK pathway is correlated with down-regulation of MMP-9 secretion induced by TNF-?? in human keratinocytes. *Exp. Cell Res.* **290,** 108–119 (2003).
23. Fan, G. *et al.* Knocking the NT4 gene into the BDNF locus rescues BDNF deficient mice and reveals distinct NT4 and BDNF activities. *Nat. Neurosci.* **3,** 350–7 (2000).
24. Zhou, L. J. *et al.* Limited BDNF contributes to the failure of injury to skin afferents to produce a neuropathic pain condition. *Pain* **148,** 148–157 (2010).
25. Ichikawa, H. *et al.* Masseteric nerve injury increases expression of brain-derived neurotrophic factor in microglia within the rat mesencephalic trigeminal tract nucleus.

Cell. Mol. Neurobiol. **31,** 551–559 (2011).

26. English, A. W., Cucoranu, D., Mulligan, A., Rodriguez, J. a & Sabatier, M. J. Neurotrophin-4/5 is implicated in the enhancement of axon regeneration produced by treadmill training following peripheral nerve injury. *Eur. J. Neurosci.* **33,** 2265–2271 (2011).

27. Salo, P. T. & Theriault, E. Number, distribution and neuropeptide content of rat knee joint afferents. *J. Anat.* **190 (Pt 4,** 515–522 (1997).

28. Hanesch, U. & Heppelmann, B. A simple method for a specific retrograde labelling of dorsal root and sympathetic ganglion cells innervating the knee joint of the cat. *J. Neurosci. Methods* **63,** 55–59 (1995).

29. Goetz, J. J. & Trimarchi, J. M. Single-cell Profiling of Developing and Mature Retinal Neurons. *J. Vis. Exp.* **0,** 1–7 (2012).

30. Lindqvist, N., Vidal-Sanz, M. & Hallböök, F. Single cell RT-PCR analysis of tyrosine kinase receptor expression in adult rat retinal ganglion cells isolated by retinal sandwiching. *Brain Res. Protoc.* **10,** 75–83 (2002).

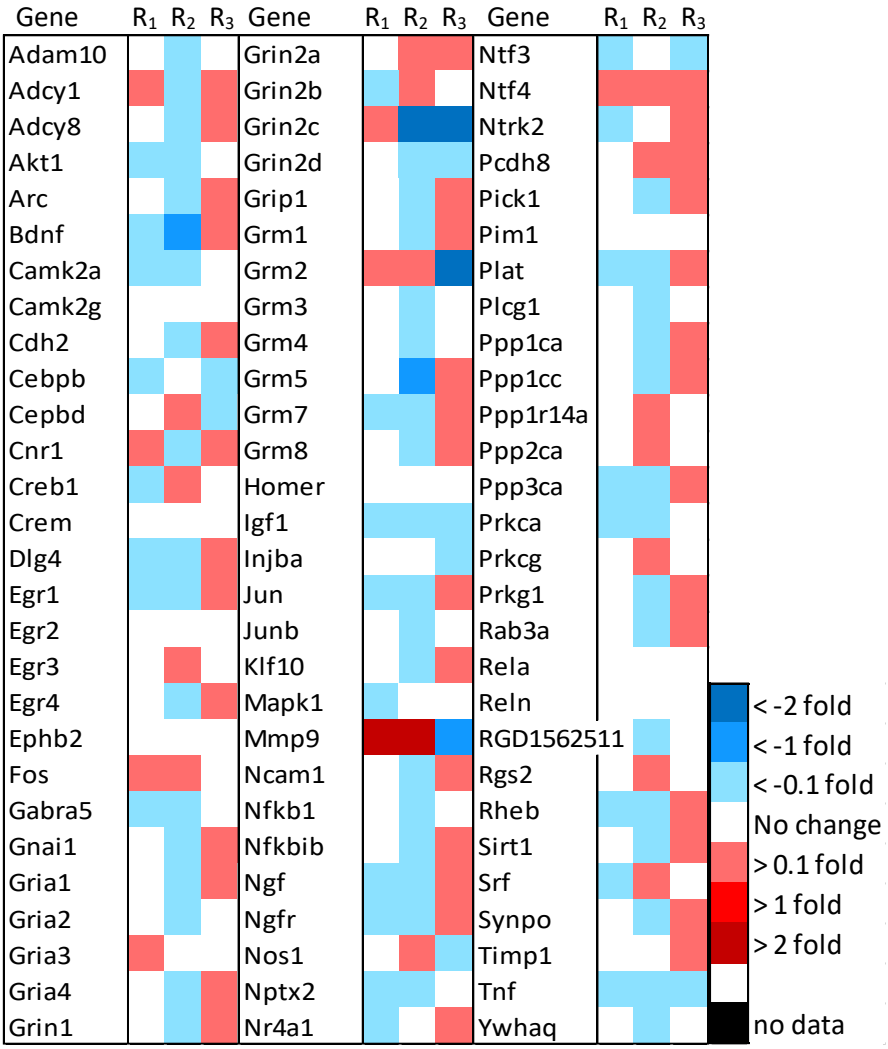

Figure 1. Heatmap of gene expression in DRGs of CCL-lesioned rats.

Fold-change between the DRGs ipsilateral and contralateral to operation are represented as colors on a heat map. Fold changes were calculated from $2^{-\Delta\Delta Ct}$. The labeled columns to the left of the maps indicate the gene of interest. Each column represents the data from one rat. A key is provided in the bar on the right. Blue squares indicate genes that were more highly expressed in the contralateral side (negative fold change in the ipsilateral side), and red squares indicate genes that were more highly expressed on the operated side. White squares indicate no change, and black squares indicate samples where data could not be obtained.

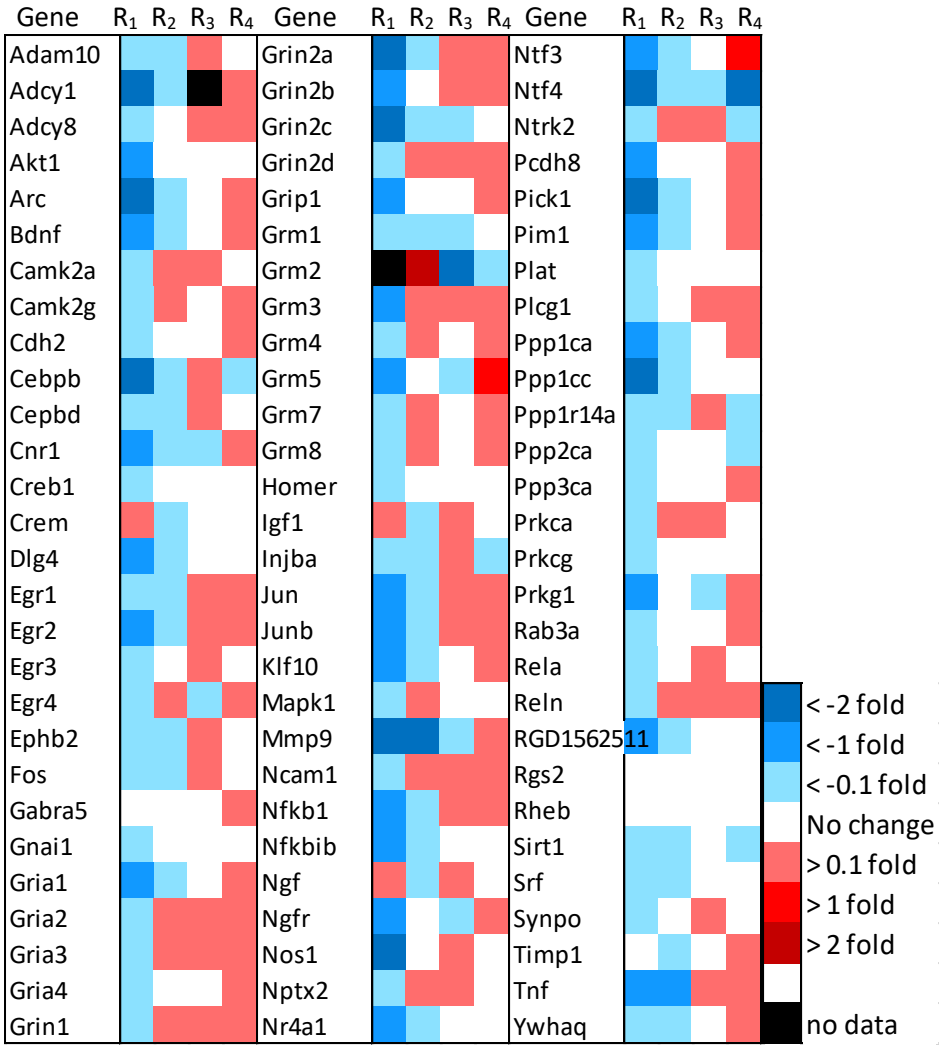

Figure 2. Heatmap of gene expression in DRGs of sham-operated rats.

Fold-change between the DRGs ipsilateral and contralateral to operation are represented as colors on a heat map. Fold changes were calculated from $2^{-\Delta\Delta Ct}$. The labeled columns to the left of the maps indicate the gene of interest. Each column represents the data from one rat. A key is provided in the bar on the right. Blue squares indicate genes that were more highly expressed in the contralateral side (negative fold change in the ipsilateral side), and red squares indicate genes that were more highly expressed on the operated side. White squares indicate no change, and black squares indicate samples where data could not be obtained.

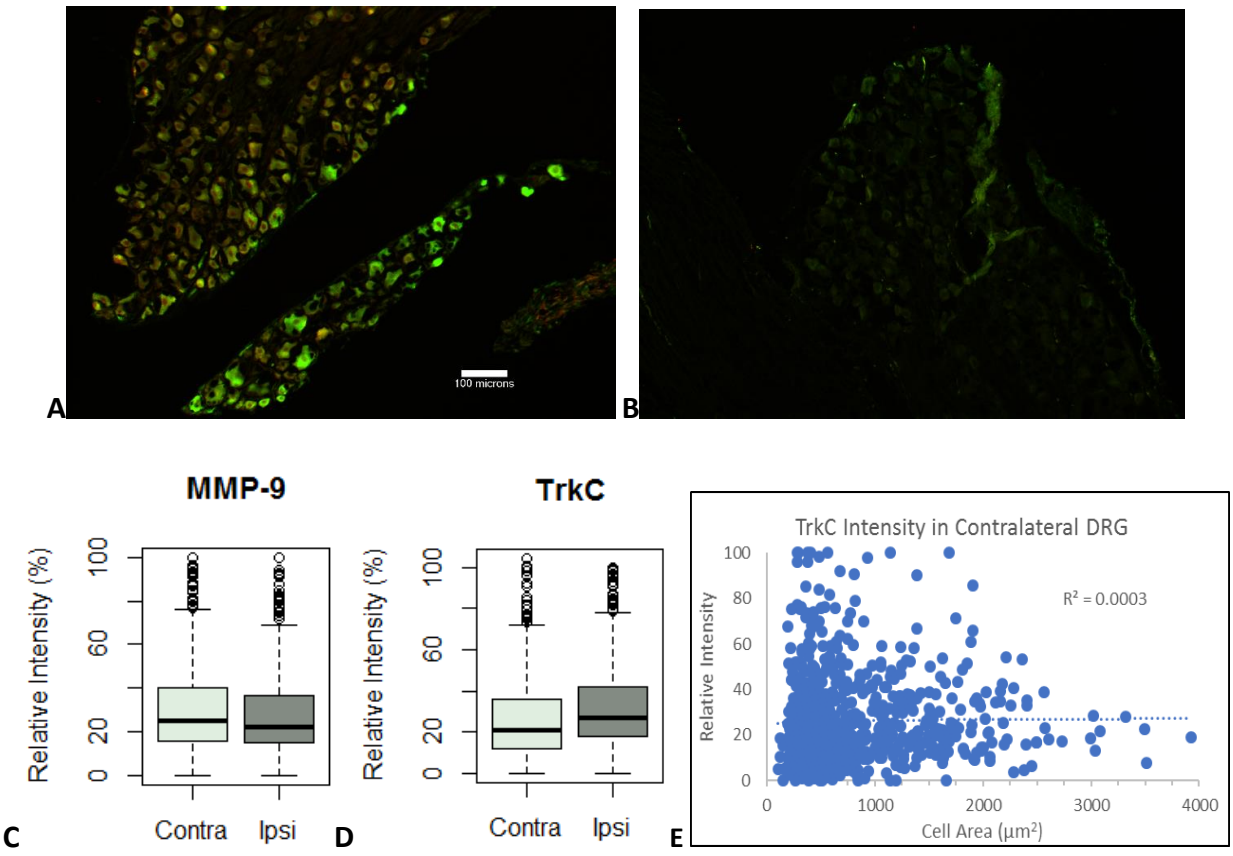

Figure 3. Immunohistochemistry for DRG ipsilateral and contralateral to knee lesions

Sections from L4 DRG of rats with surgical lesions to the CCL on the right knee. MMP-9 staining (red) and TrkC staining (green) are shown here from DRG contralateral (A) and ipsilateral (B) to the lesion. (C) Relative intensity for MMP-9 was slightly but significantly lower in DRG innervating the lesioned knee ($p = 0.0129$). (D) The mean relative intensity of TrkC staining was significantly higher in the DRG ipsilateral to knee lesions ($p < 0.0001$). (E) In the internal control (contralateral) DRG sections, there was no relationship between size and the relative intensity of TrkC staining, contrary to what was expected. Scale bar in A and B represents 100 µm.

CHAPTER 3

A COMBINED PROTOCOL FOR THE RETROGRADE TRACING AND SINGLE-CELL RNA COLLECTION OF CELLS IN PROPRIOCEPTIVE CIRCUITS

Abstract

Changes in proprioceptive circuitry induced by injury or inflammation are poorly understood. Most of what work has been done on the molecular level has been focused on specific genes or proteins. Few studies have looked at proprioceptors and γ-motoneurons (γ-MNs) to examine broadly what phenotypic changes happen in response to injury. We propose a method coupling the retrograde labeling of cells innervating the injury site, with tissue dissociation and single cell isolation for gene expression analysis. We put forth a protocol for DiI tracing of cells, followed by dissociation of dorsal root ganglia (DRG) and spinal cord ventral horn in enzyme solutions and single-cell harvesting in lysis buffer.

Introduction

Altered sensitivity in a region of the body is a frequent consequence of injury and inflammation[1–8]. This can be seen both in studies on pain and on proprioception (the sense of the position or change in position of body parts), and the effects can be acute, sustained, or chronic. Still very little is understood about these changes or their mechanisms. For instance, various injuries can lead to excessive sensitivity of the affected region to pain (hyperalgesia)[3,5–7,9–11], or a painful response not appropriate to the stimulus (allodynia)[3,5,6,10,11]. In regards to proprioception, human patients with knees mechanically stabilized knees after anterior cruciate ligament (ACL) injuries often still report feelings that the knee is unstable[12,13]. In both human

and dog subjects with ruptured cruciate ligaments, alterations to the hamstring reflex, a response that stabilizes the knee, are consistently observed in electromyograms (EMG)[12,14].

Nociceptive and proprioceptive pathways both involve complex processing at various levels of the nervous system. However, one key way to examine changes to these pathways is to look at cells directly interacting with the affected tissue in injury and inflammation models. That is, it is critical to understand what is happening in cells that innervate the site of the injury. Furthermore, in the absence of a visible marker distinguishing cell type, the ability to assess phenotypes at the level of a single cell can allow for *post-hoc* parsing of data based on cell-type specific gene expression (if multiplex analysis is used). To this end, we propose a model for using a retrograde tracer, DiI, to locate the neurons connected to the tissue of interest and to subsequently isolate whole cells for studies in gene expression using enzymatic tissue dissociation. For the purposes of proprioception, this also includes the gamma-motoneurons (γ-MNs) in the spinal cord, as they modulate tension, and thus sensitivity, in muscle spindles.

Comparison with Other Techniques

Other tracing studies

The reason for using retrograde axonal tracers is to identify neurons based on their target tissue. These types of tracers have been used to study the amount of innervation to a given region[15–17], the locations of innervation cell bodies[18,19] , and the changes these cell bodies incur after experimental events[4,7,10,20–22]. DiI was chosen for the tracer due to its relatively easy uptake and transport and to its nearly indefinite survival time within a live organism[23,24]. Because of this, DiI can be injected days or weeks before injury, so as not to alter the effects of the injury, and animals can be kept alive for any amount of time before harvesting.

The reason for selecting neurons by target is to determine the response of individual cells to local changes in their target tissue. Broader tracing techniques involve damaging nerves[24,25]. Though such techniques are critical in studying pain resulting from nerve damage, in this case they are undesirable both because they confound the response to changes in target tissue, and because they raise animal welfare issues due to extended survival periods.

This technique addresses questions particularly centered around the transcriptome of labeled cells. Previous studies have looked at changes in the expression of individual genes in traced cells, mostly through immunohistological techniques[7,21,25]. These studies produce thorough assessments of global expression changes, but proprioceptive circuits rely on specific neuronal subtypes. Analysis of phenotypic change in cells relating to proprioception thus necessitates the extraction of whole, individual cells.

Other single cell isolation methods

Tissue dissociation techniques have long been used to prepare cells for culturing[26–28]. The following techniques even draw from the experience from previous publications in dissociating mouse DRG[4,25–27,29–31] and spinal cord[25,28,32,33]. However, this protocol takes cells directly into an isolation and lysis step for analyzing the RNA. Several previous studies have done this as well[26,34]. The main distinction in this case is that, while most previous single-cell gene expression studies have been used for characterizing cell types or tracking development, we are tracking gene expression in response to peripheral environmental factors.

Experimental Design

The procedure adheres to the following steps. Initially, mice are injected in the biceps femoris muscle (BF, the largest and most accessible of the hamstring muscles) with solutions of DiI and DMSO under general anesthesia (Steps 1-5) and allowed to recover for 14 days to allow the fluorescent dye to reach the cell bodies of traced neurons[23]. The animals are then euthanized, and DRG are collected from the lumbar 5 and 6 levels[18,19] on the side of the animal where the injection was made, while the caudal half of the lumbar enlargement is collected from the spinal cord[18] (Steps 6-13).

Fresh tissues are dissociated using solutions of proteolytic enzymes. For spinal cord tissue, we use a solution of collagenase and dispase (Steps 14-18)[33], while DRG are dissociated using a papain solution followed by a collagenase/dispase solution (Steps 19-25)[27,29]. Cells are then picked from a petri dish and placed individually into TCL lysis buffer, and RNA is extracted using RNAClean XP beads from Agencourt (Steps 26-34). Afterward, cDNA is reverse transcribed from the samples and amplified using a SMART-Seq kit from Clontech (Steps 35-38)[35]. This can then go on to be used for RNA-Seq (Steps 39-46). The basic design for the protocol is laid out as a flowchart in Figure 1.

Materials

Reagents/buffers

- Agencourt AMPure XP beads (Beckman-Coulter A63880)
- Agencourt RNAClean XP beads (Beckman-Coulter A63987)
- Bovine serum albumin (BSA) powder (Sigma-Aldrich A7906)
- Buffer TCL 2× (Qiagen 1070498)

- Collagenase, Type 1 100 mg (Worthington LS004194)
- L-Cysteine (Sigma C7352)
- DiI (Aldrich 468495)
- Dimethyl Sulfoxide (DMSO, Sigma-Aldrich D8418)
- Dispase II (Sigma-Aldrich D4693)
- Ethylenediaminetetraacetic acid (EDTA, Sigma-Aldrich E9884)
- Ethanol, nuclease-free 100% (EtOH 100%, Sigma-Aldrich)
- Ethanol spray 70% (EtOH 70%)
- Hanks Buffered Salt Solution (HBSS) 1× (Gibco 14170)
- 4-(2-hydroxyethyl)-1-piperazineethanesulfonic acid (HEPES, Sigma-Aldrich H3375)
- Isoflurane (VetOne 1-3985-528-60)
- Papain (Roche 10108014001)
- Phosphate buffered saline (PBS) tablets (Life Technologies 003002)
- PBS 10× nuclease-free (Ambion AM9624)
- RNase*ZAP* (Ambion AM9780
- Saline, sterile 0.9%
- Water, nuclease-free (nuclease-free H_2O, Invitrogen 10977-015)
- SMART-Seq v4 Ultra Low Input RNA Kit for Sequencing (Clontech Laboratories 634898)

Equipment

- C57BL/6 mice (Charles River Laboratories)
- Disposable Bench Cover

- SoftHeat warming pad (Kaz)
- Vaporizer with induction box (SurgiVet Model 100)
- SomnoSuite small animal anesthesia system (Kent Scientific)
- Clippers (Wahl)
- Hamilton Syringe, 10 µL 31-guage (Hamilton 80308)
- Nolvasan pads
- Oxygen tank
- CO_2 chamber
- Scissors, medium surgical
- 1-pair small spring scissors (Excelta 366, Fisher 17-467-496)
- 1-pair fine tip tapered forceps (Fisher 16-100-113)
- 1-pair fine tip reverse action forceps (Fisher 16-100-126)
- Scalpel, size 10 (Miltex 4-110)
- Centrifuge (Eppendorf 5417 C)
- Warm water bath (37° C)
- Pasteur pipettes, glass (Fisher 13-678-20A)
- 2mL Rubber bulb (Fisher 03-448-24)
- Petri dishes, sterile plastic
- Inverted fluorescent microscope (Nikon)
- 2 µL - Microcapillary tubes, heated and pulled to make 2 microcapillary pipettes each (Drummond 1-000-0020)

- Aspirator tube assembly (Sigma Aldrich A5177)
- Laminar Flow PCR cabinet (Streamline)
- DynaMag (Invitrogen 49-2025)
- Thermocycler, Veriti 96-well (Applied Biosystems)

Setup

Stock solutions

Make up non-sterile PBS solution (for washing dissection sites) by adding 1 tablet to each 100 mL of filtered or nuclease-free H_2O.

Prepare 10 % DiI in DMSO solution by adding 100 mg of DiI powder to 800 µL of DMSO. Vortex the mixture until it is dissolved. Add DMSO to bring the total volume up to 1 mL. Do this procedure in a dark or dim room, and keep the stock solution protected from light at -20° C.

Make up 1 M stock solution of L-cysteine the day before dissociations by adding 606 mg L-cysteine powder to 5 mL of nuclease-free H_2O. Vortex the mixture thoroughly until dissolved. Store this at 4° C. Do this the day before dissociations, since L-cysteine in solution will oxidize into cystine and precipitate.

Make up stock EDTA in a small beaker by adding 7.306 g of EDTA powder to 25 mL of nuclease-free H_2O on a magnetic-stir hot plate at moderate heat and with a stir bar active. Every few minutes, add drop or two of 1 M NaOH until the EDTA is completely dissolved. Adjust the pH to ~8.0, move the solution to a 50 mL conical tube and add nuclease-free H_2O until the total volume is 50 mL. Store the solution at 4° C.

Make stock HEPES by adding 2.383 g HEPES powder to 8 mL nuclease free H_2O, and vortex the mixture until it is dissolved. Add nuclease-free H_2O to bring the volume up to 10 mL. Store the solution at 4° C.

Prepare 62.5× (15,625 U/mL) collagenase I by adding the appropriate amount of HBSS to the collagenase powder (Units/weight for the batch will be given on the label). Filter this into sterile microcentrifuge tubes or PCR tubes and store them at -20° C.

Prepare 100× (240 U/mL) dispase II stock following the same steps as with collagenase I.

In advance, make up stock 5% BSA stock by adding 0.25 g of BSA powder to 3 mL of nuclease-free PBS diluted to 1× in a conical tube. Vortex or turn the conical tube gently until the BSA is dissolved. It is easiest to add portions of the BSA at a time. Once this has been dissolved, allow the solution to settle in a 4° C cooler or centrifuge it to break up the bubbles. Add PBS to bring the volume up to 5 mL. Put the solution in a Luer-lock syringe with a 0.2 µm filter attached, and use it to distribute the solution into microcentrifuge tubes. Store the stock buffer at -20° C.

Workspace

Clean all workspaces before using. Wipe down areas with 70% EtOH spray for all procedures. When working with RNA or preparing materials for RNA extraction, use a dedicated workspace if possible. If one is not available, wipe down equipment and work areas with RNase*ZAP*.

Equipment

Heat and pull microcapillary tubes in a needle puller to produce microcapillary pipettes. Be sure to use the same machine with the same settings every time. Use one pipette to take up

4.5 µL of premeasured H_2O and mark the place where the water ends. Use this reference to mark the 4.5 µL point on the other microcapillary pipettes.

Protocol

Tracer dye injections

1. Mix up the dye solution by adding stock DiI/DMSO solution to sterile H_2O (1:10). Vortex the solution thoroughly (final concentration of 1% DiI and 10% DMSO). If it does not completely dissolve, it can be further dissolved through sonication.
2. Place mouse in induction box. Induce anesthesia with 2% isoflurane at 2% air replacement per minute. When the mouse is thoroughly unconscious, place on the warmed bench mat with a heating pad and put the Somnosuite nose cone over its face. Initiate airflow to the nosecone at 140 to 170 mL/min. Shave the right leg of the mouse. Wash with Nolvasan and then with alcohol to sterilize the area. While the mouse is anesthetized, draw 5 µL of the dye solution into the Hamilton syringe. (*Troubleshooting*: If the dye solution is not being drawn up into the syringe, or undissolved flecks are visible, sonicate the sample again.)
3. Using a razor blade, scissors ends, or fine scalpel, make a small incision near the lower caudal part of the lateral thigh near the back of the knee joint (Fig 2). Be sure not to cut through the fascia.
4. Move the skin until the incision is over the back of the BF about halfway up. Insert the Hamilton syringe at around a 20-degree angle to the surface, going proximally and parallel to the back side of the BF triangle (Fig 2) until the needle is 5.5 to 6 mm in. This should bring it to a point of the BF near the insertion in the hip, around 2 mm deep.

Slowly inject 3 to 4 µL of dye solution. Hold the syringe in place for 1 to 2 minutes before slowly removing. Move the incision window slightly closer to the back of the knee. Insert the needle going anterior and slightly proximally (again, at a 20-degree angle to the surface), until the needle is 4.5 to 5 mm deep. Inject as before. (*Helpful Tip*: DMSO can cause acute and transient muscle spasms. These are minor, and end before the animal regains consciousness. We have observed that these mild spasms are a helpful guide to ensure you have injected the correct muscle.)

5. When finished, wash the wound with sterile saline from a syringe. Place the mouse in a warmed cage until it regains consciousness.

Dissections

6. Before dissections, prepare working solutions and buffers for tissue dissociation. Add 100 µL of HEPES stock to 9.9 mL HBSS to supplement the HBSS with 10 mM HEPES[34]. Prepare 0.1% BSA by adding 200 µL 5% BSA stock to 9.8 mL nuclease-free 1× PBS in a conical tube. For collagenase/dispase, add 48 µL of collagenase stock solution to 2.9 mL of HBSS/HEPES, then add 30 µL of dispase II stock solution. The working concentrations should be 250 U/mL collagenase I and 2.4 U/mL dispase II. For a working papain solution, add 12 µL of cysteine stock and 12 µL of EDTA stock to 2.2 mL of HBSS/HEPES. Next add 160 µL of stock papain. Working concentrations will be 20 U/mL papain, 5 mM cysteine, and 0.5 mM EDTA. Allow the papain solution to incubate at room temperature for 30 minutes before using. (*Variation*: All solutions can be scaled up for larger amounts of tissue.)

7. Place mouse in chamber and turn on CO_2 to replace 20% of air per minute. Wait until respiration has ceased for a minute. Turn off CO_2 and remove mouse from chamber. Place a pen at the back of the head and hold the tail. In a single motion, press down and forward on the neck and pull up and back on the tail to break the neck. Check to make sure cervical spine has been dislocated.
8. Shave the back of the mouse and remove all excess hair. Cut open the ventral side of the animal with several paper towels underneath the animal, and cut the heart. This allows blood to drain out the ventral side of the animal so that it will cause fewer complications in the dissection of the spine.
9. Spray the back of the animal with 70% EtOH. Cut skin across and pull open to reveal the back. Cut the skin along the back to fully expose the spine.
10. Cut across and into the spinal column in upper to mid thoracic level. Lift up the spine using forceps and cut the top of the vertebra and surrounding tissue on either side. Move along and alternate between sides. Go until the lower thoracic and upper lumbar have been exposed. Locate the 13th thoracic (T13) vertebral body by finding the last floating rib. Count to the appropriate lumbar segments and remove the DRG from the 5th and 6th (L5 and L6) segments (Fig 3).
11. Place DRGs in PBS or HBSS and, under spectacle-mounted magnifying glasses (loupes) or a dissecting microscope, trim them. Place them in tubes of HBSS and put them on ice.
12. Keep spinal cord from drying using PBS. Locate the L2-L6 segments (From caudal T11 to rostral L1 vertebral bodies ~8mm long[36], Fig 3). Carefully cut out the section, place in PBS or HBSS.

13. Cut the spinal cord along the midline, and set aside the left side. Turn the right side over so that the dorsal horn can be cut off. Discard dorsal portion. Cut the portion of interest into 4 equal segments (2mm lengths). Collect the caudal two segments in an HBSS tube and place them on ice.

Dissociation

Spinal cord

14. Using forceps, carefully move the length of spinal cord and place it on a glass slide in a petri dish. Keep it hydrated with HBSS. Using a scalpel, cut down the midline of the spinal cord, and discard the tissue from the unlabeled side. Carefully trim off the dorsal half of the spinal cord, and trim off white matter. Place the isolated ventral horn in 1 mL of pre-warmed HBSS. (*Variation*: The volume of HBSS may be increased as needed if samples are being pooled.)
15. Spin the sample at 1000 rpm for 1 minute. Aspirate the HBSS and replace it with 1100 µL of a pre-warmed collagenase/dispase solution and place it in the 37° C water bath. Gently vortex the sample at a low setting every 5 minutes to keep the sample suspended (tapping to disrupt the tissue can introduce air bubbles, which can damage cells). Triturate with a glass micropipette and a rubber bulb 10 times halfway through the incubation.
16. After 40 minutes, remove the sample from the heat bath and triturate the sample with a glass micropipette 10 times to fully dissociate the cells.

17. Centrifuge the sample at 3600 rpm for 3 minutes. Aspirate the supernatant and resuspend the pellet in 1 mL of 37° C HBSS. (*Troubleshooting*: If there is a trail of cells along the of the tube, centrifuge it for one or two more minutes.)
18. Centrifuge the sample again at 3600 rpm for 3 minutes. Aspirate the supernatant and resuspend the sample in 500 µL BSA solution. Let the suspension sit for 1 minute, allowing large, undissociated debris to settle to the bottom, then transfer 400 µL to a new tube. Add 300 µL of BSA to the old tube, resuspend the sample, and allow it to settle again before transferring 300 µL to the new tube. Do this once more with 300 µL of BSA. The new sample tube should have approximately 1 mL suspension. (*Variation*: These volumes can be scaled up if samples are being pooled.)

Dorsal root ganglion

19. Place DRG L3 and L4 in a petri dish in HBSS. Using forceps and small spring scissors, carefully remove the meninges and any remaining nerve tissue. Using a pipette, carefully draw up the DRG and place it in 1 mL of 37° C HBSS.
20. Spin the sample at 1000 rpm for 1 minute. Aspirate the HBSS and replace it with 1200 µL of a pre-warmed papain solution and place it in the 37° C water bath. Vortex the sample gently on a low setting every 5 minutes for 20 minutes.
21. Triturate the sample 10 times with a glass micropipette, then spin it at 2300 rpm for 4 minutes. (*Troubleshooting*: If there is a trail of cells along the of the tube, centrifuge it for one or two more minutes.)
22. Aspirate the supernatant and resuspend the pellet in 1400 µL of Collagenase/Dispase solution. Replace the sample in the 37° C bath for 20 minutes.

23. Triturate the sample 10 times, then centrifuge it at 2300 rpm for 4 minutes. (*Troubleshooting*: If there is a trail of cells along the of the tube, centrifuge it for one or two more minutes.)
24. Aspirate the supernatant and resuspend the pellet in 1300 µL or 37° C HBSS. Centrifuge the sample at 2300 rpm for 4 minutes. (*Troubleshooting*: If there is a trail of cells along the of the tube, centrifuge it for one or two more minutes.)
25. Centrifuge the sample again at 3600 rpm for 3 minutes. Aspirate the supernatant and resuspend the sample in 250 µL BSA solution. Let the suspension sit for 1 minute, then transfer 200 µL to a new tube. Resuspend the sample in the original tube with 200 µL BSA, allow it to settle for 1 minute, then transfer 200 µL to the new tube. Do this once more with 200 µL of BSA. The new sample tube should have approximately 600 µL suspension. (*Variation*: These volumes can be scaled up if samples are being pooled.)

Single cell isolation and RNA extraction

26. Bring the cell suspension and pre-measured PCR tubes of lysis buffer to an inverted fluorescent microscope. Place 6 mL of 0.1% BSA solution into a petri dish, or enough to cover the bottom. Pipette 500 µL of cell suspension into the petri dish. Place it on the stage of the microscope (with the lights turned off) and allow it to settle for 5 minutes. During this time prepare TCL for cell collection by adding 1 µL β-Mercaptoethanol to 49 µL 2× TCL and place 4.5 µL of the solution into each PCR tube, keep covered and on ice. (*Variation*: The lid of a multi-well plate can be used in place of a petri dish if this is preferred. If more cells are to be harvested, prepare more TCL buffer.)

27. Turn on the fluorescence with a red filter setting (TRITC filter set). Locate a cell that fluoresces red, and then switch to bright-field illumination.
28. Take the microcapillary pipette and place it in the tube apparatus. Place the other end of the apparatus in your mouth, and press against it with the tongue (this keeps pressure inside the tube so that capillary action does not fill up the pipette before picking the cell). Carefully move the pipette until it is next to the cell in the objective, then release the pressure in the tube by releasing your tongue just long enough to pick up the cell. From another container, take in BSA until it has reached the marker on the microcapillary pipette. **Critical step**
29. From a clean tube of BSA, fill the pipette. Putting pressure on the tube, eject the cell and solution carefully into a tube of pre-measured lysis buffer (still on ice). Cap the tube and keep it on ice.
30. Repeat steps 2 through 4 until the desired number of labelled cells have been collected. If there are not enough labelled cells in the dish initially, add the rest of the sample to the petri dish.
31. When the desired number of cells has been collected, move the tubes to an RNase-free work area and remove from the ice. Allow the cells to incubate at room temperature for 30 minutes.
32. Add 16.2 µL (1.8 volumes) of Agencourt RNAClean XP solution to each tube. Pipette gently up and down 10 times. Incubate for 3 to 5 minutes at room temperature. Then place the tubes in a magnet for 5 minutes. If the solution has become clear, remove the

supernatant carefully. While the samples are incubating, prepare 70% ethanol from nuclease-free H_2O and nuclease-free 100% EtOH.

33. Add 200 µL of 70% Nuclease-free ethanol to each tube, and allow to sit at room temperature for 30 seconds before aspirating. Repeat this step two more times.
34. Allow the reaction to air dry. This should take around 10 minutes. When it is dry, add 10 to 15 µL Ultrapure H_2O and pipette up and down 10 times. Take the samples off of the magnet and put them on ice. **Critical step**

cDNA synthesis

35. Add 1 µL of reaction buffer to each RNA sample. Place samples on ice. With samples on ice, add 2 µL of 3' SMART-Seq CDS Primer IIA. Vortex or pipette the samples gently. Briefly spin down the samples on a small centrifuge.
36. Incubate the samples in a preheated, hot-lid thermocycler at 72°C for 3 minutes. Immediately place samples on ice for 2 minutes. Preheat the thermocycler to 42° C. In the meantime, prepare the Master Mix according to manufacturer instructions.
37. Add 2 µL of SMARTScribe Reverse Transcriptase to Master Mix just before use. Then add 7.5 µL Master Mix to each reaction.
38. Place samples immediately in Thermocycler and run the following program
    - 42°C for 90 minutes
    - 70°C for 10 minutes
    - 4°C indefinitely

    Place the samples on ice afterward. (**Pause point**: From here, samples can be kept overnight at 4° C.)

cDNA amplification and purification

39. Remove samples from cooler. Prepare PCR master mix and add 30 µL of it to each sample. Mix and briefly spin them.
40. Place tubes in preheated thermocycler and run the following program
    - 95°C for 1 minute
    - 15 X
        - 98°C for 10 seconds
        - 65°C for 30 seconds
        - 68°C for 3 minutes
    - 72°C for 10 minutes
    - 4°C indefinitely
41. Add 1 µL of 10X Lysis Buffer to each sample. Then add 50 µL of Agencourt AMPure XP beads to each sample. Pipette each one up and down 10 times.
42. Incubate the samples at room temperature for 8 minutes. Briefly spin and place samples in the magnet for 5 minutes, or until the beads have separated out. Remove the supernatant. While the samples are incubating, prepare 80% ethanol from nuclease-free H_2O and nuclease-free 100% EtOH.
43. Add 200 µL of Nuclease-Free 80% Ethanol to each sample carefully. Incubate 30 seconds before carefully removing the ethanol. Repeat this step one more time.
44. Incubate the pellet to sit at room temperature for 2 to 2 ½ minutes, when the pellet has just barely dried. **Critical step**

45. Add 17 µL of nuclease-free H_2O, remove the samples from the magnet and gently pipette several times. Incubate samples at room temperature for 2 minutes.
46. Briefly spin the samples and place them back on the magnet until the solution has become clear. Then carefully remove the supernatant and place it in a new tube that has been appropriately labeled for the contents. Discard the tube containing the beads.

Discussion

Verification of steps in the protocol

The efficacy of the tracing procedure was verified histologically. DRG samples were briefly fixed in 4% paraformaldehyde, cryoprotected in graded sucrose solutions (15%, 20%, 30%, 12 hours each), and flash frozen in O.C.T. (Tissue-Tek). Using a cryostat (Thermo Scientific), 10 µm-thick sections of L4, L5, and L6 DRG and 30 µm-thick spinal cord samples were collected onto glass Superfrost plus slides (VWR). Labeled cells were located in L4 and L5 DRG (Fig 4). Likewise, labelled motoneurons were found in the ventral horn of sections from the caudal half of lumbar enlargement spinal cord. These were also located in the same region of the ventral horn as BF traced neurons traced by Bacskai and colleagues[18].

Due to events beyond our control, we were unable to complete the protocol in full. Tests were performed on tissue from untraced mice to compare the enzyme mixtures and dissociation protocols used in previous techniques (Fig 5). We were unable, however, to obtain a large number of neuron sized cells (at least 250 μm^2)[7,15,37,38] in any of the samples. This is likely because of the fact that these cells, due to time constraints around housing time of the animals, were stored in RNA*later* at -80° C, allowing us to dissect all rats in one day and dissociate on a later date.

Furthermore, we were not able to verify the RNA isolation or the cDNA output from isolated cells. However, we did test the quality of cDNA using rat DRG cells dissociated with papain followed by collagenase/dispase. As with our mouse samples, the rat tissue had also been stored in RNA*later* at -80°C. During the cDNA synthesis and amplification steps, one tube was prepared using 30 pg of control RNA (from SMART-Seq kit) for each of three test runs as positive controls. The cDNA samples were analyzed on High Sensitivity DNA chips (Agilent) on an Agilent 2100 Bioanalyzer. According to personal correspondence with ClonTech technical service, 10 pg of high-integrity RNA should yield 3.4 ng of cDNA. One sample yielded almost no cDNA, even in the control well, whereas the others yielded approximately 1.67 ng total (Fig 6a) and 9.43 ng total. One cell from the same sample as the 1.67 ng control yielded approximately 1.49 ng total (Fig 6b). This suggests that the synthesis and amplification step is working most of the time, and that some cells are producing cDNA, but there is still a problem either capturing cells or with the extraction of RNA. However, previous studies have accomplished this combination of protocols[35].

Applications of the protocol and possible future steps

This technique has potential for assessing gene-expression responses of neurons to various peripheral conditions. Pain studies, for instance, would be able to focus on the response of a small number of cells to localized injuries. In one study, neurons were traced with DiI prior to the injection sites being inflamed using an adjuvant[8]. Electrophysiological experiments on the dissociated neurons revealed increased excitability in the inflamed group compared to the control, but they did not look at gene expression. Other studies have revealed upregulations of sodium channels to be involved in increased pain sensitivity after inflammation[5,6], but did not

trace the cells in question. Another experiment showed evidence that increased sensitivity in cells traced from the knee involved more readily phosphorylated ERK[7].

This technique also has broad potential for studying alterations in proprioception. Little has been done to assess changes in proprioception after injury, but an increase in sensitivity has been associated with increased voltage-gated sodium channels (specifically $Na_v1.8$) in Aβ fibers, which receive signals from non-adapting stretch receptors[5]. Additionally, since the technique involves tracing the muscle, it allows investigators to assess changes in gamma motoneurons. This is important because it can show responses to synergistic changes as well. For instance, hamstring gamma motoneurons have been shown to respond reflexively to stretches in the cruciate ligament[39], thus playing a role in stabilization of the knee joint.

References

1. Radhakrishnan, R., Moore, S. A. & Sluka, K. A. Unilateral carrageenan injection into muscle or joint induces chronic bilateral hyperalgesia in rats. *Pain* **104,** 567–577 (2003).
2. Wu, Q. & Henry, J. L. Changes in Abeta non-nociceptive primary sensory neurons in a rat model of osteoarthritis pain. *Mol. Pain* **6,** 37 (2010).
3. Jin, S.-X., Zhuang, Z.-Y., Woolf, C. J. & Ji, R.-R. p38 Mitogen-Activated Protein Kinase Is Activated After a Spinal Nerve Ligation in Spinal Cord Microglia and Dorsal Root Ganglion Neurons and Contributes To the Generation of Neuropathic Pain. *J. Neurosci.* **23,** 4017–4022 (2003).
4. Lolignier, S. *et al.* Nav1.9 channel contributes to mechanical and heat pain hypersensitivity induced by subacute and chronic inflammation. *PLoS One* **6,** 1–11 (2011).
5. Belkouch, M. *et al.* Functional up-regulation of Nav1.8 sodium channel in Aβ afferent fibers subjected to chronic peripheral inflammation. *J. Neuroinflammation* **11,** 45 (2014).
6. Joshi, S. K. *et al.* Involvement of the TTX-resistant sodium channel Nav 1.8 in inflammatory and neuropathic, but not post-operative, pain states. *Pain* **123,** 75–82 (2006).
7. Seino, D. *et al.* The role of ERK signaling and the P2X receptor on mechanical pain evoked by movement of inflamed knee joint. *Pain* **123,** 193–203 (2006).
8. Flake, N. M. & Gold, M. S. Inflammation alters sodium currents and excitability of temporomandibular joint afferents. *Neurosci. Lett.* **384,** 294–299 (2005).
9. Ji, R. R., Samad, T. A., Jin, S. X., Schmoll, R. & Woolf, C. J. p38 MAPK activation by NGF in primary sensory neurons after inflammation increases TRPV1 levels and maintains heat

hyperalgesia. *Neuron* **36,** 57–68 (2002).

10. Zhou, L. J. *et al.* Limited BDNF contributes to the failure of injury to skin afferents to produce a neuropathic pain condition. *Pain* **148,** 148–157 (2010).
11. Nascimento, G. C., Rizzi, E. & Gerlach, R. F. Expression of MMP-2 and MMP-9 in the rat trigeminal ganglion during the development of temporomandibular joint inflammation. **46,** 956–967 (2013).
12. Beard, D. J., Kyberd, P. J., Fergusson, C. M. & Dodd, C. a. Proprioception after rupture of the anterior cruciate ligament. An objective indication of the need for surgery? *J. Bone Joint Surg. Br.* **75,** 311–315 (1993).
13. Tyler, T. F., McHugh, M. P., Gleim, G. W. & Nicholas, S. J. Association of KT-1000 measurements with clinical tests of knee stability 1 year following anterior cruciate ligament reconstruction. *J. Orthop. Sports Phys. Ther.* **29,** 540–545 (1999).
14. Hayes, G. M., Granger, N., Langley-Hobbs, S. J. & Jeffery, N. D. Abnormal reflex activation of hamstring muscles in dogs with cranial cruciate ligament rupture. *Vet. J.* **196,** 345–350 (2013).
15. Salo, P. T. & Theriault, E. Number, distribution and neuropeptide content of rat knee joint afferents. *J. Anat.* **190 (Pt 4,** 515–522 (1997).
16. Gómez-Barrena, E., Nuñez, A., Ballesteros, R., Martinez-Moreno, E. & Munuera, L. Anterior cruciate ligament reconstruction affects proprioception in the cat's knee. *Acta Orthop. Scand.* **70,** 185–93 (1999).
17. Freeman, M. a & Wyke, B. The innervation of the knee joint. An anatomical and histological study in the cat. *J. Anat.* **101,** 505–532 (1967).

18. Bácskai, T., Rusznák, Z., Paxinos, G. & Watson, C. Musculotopic organization of the motor neurons supplying the mouse hindlimb muscles: A quantitative study using Fluoro-Gold retrograde tracing. *Brain Struct. Funct.* **219,** 303–321 (2014).

19. Mohan, R., Tosolini, A. P. & Morris, R. Targeting the motor end plates in the mouse hindlimb gives access to a greater number of spinal cord motor neurons: An approach to maximize retrograde transport. *Neuroscience* **274,** 318–330 (2014).

20. Li, S. *et al.* The transcriptional landscape of dorsal root ganglia after sciatic nerve transection. *Sci. Rep.* **5,** 16888 (2015).

21. Rau, K. K. *et al.* Cutaneous tissue damage induces long-lasting nociceptive sensitization and regulation of cellular stress- and nerve injury-associated genes in sensory neurons. *Exp. Neurol.* **283,** 413–427 (2016).

22. Zhu, Y., Dua, S. & Gold, M. S. Inflammation-induced shift in spinal $GABA_A$ signaling is associated with a tyrosine kinase-dependent increase in $GABA_A$ current density in nociceptive afferents. *J. Neurophysiol.* **108,** 2581–93 (2012).

23. Choi, D., Li, D. & Raisman, G. Fluorescent retrograde neuronal tracers that label the rat facial nucleus: A comparison of Fast Blue, Fluoro-ruby, Fluoro-emerald, Fluoro-Gold and DiI. *J. Neurosci. Methods* **117,** 167–172 (2002).

24. Novikova, L., Novikov, L. & Kellerth, J. O. Persistent neuronal labeling by retrograde fluorescent tracers: A comparison between Fast Blue, Fluoro-Gold and various dextran conjugates. *J. Neurosci. Methods* **74,** 9–15 (1997).

25. Seo, T. B. *et al.* ERK1/2-Mediated Schwann Cell Proliferation in the Regenerating Sciatic Nerve by Treadmill Training. *J. Neurotrauma* **26,** 1733–1744 (2009).

26. Li, C.-L. *et al.* Somatosensory neuron types identified by high-coverage single-cell RNA-sequencing and functional heterogeneity. *Cell Res.* 1–20 (2015). doi:10.1038/cr.2015.149

27. Malin, S. a, Davis, B. M. & Molliver, D. C. Production of dissociated sensory neuron cultures and considerations for their use in studying neuronal function and plasticity. *Nat. Protoc.* **2,** 152–160 (2007).

28. Yip, P. K., Kaan, T. K. Y., Fenesan, D. & Malcangio, M. Rapid isolation and culture of primary microglia from adult mouse spinal cord. *J. Neurosci. Methods* **183,** 223–237 (2009).

29. Bosmans, F., Puopolo, M., Martin-Eauclaire, M.-F., Bean, B. P. & Swartz, K. J. Functional properties and toxin pharmacology of a dorsal root ganglion sodium channel viewed through its voltage sensors. *J. Gen. Physiol.* **138,** 59–72 (2011).

30. Thériault, O. & Chahine, M. Correlation of the electrophysiological profiles and sodium channel transcripts of individual rat dorsal root ganglia neurons. *Front. Cell. Neurosci.* **8,** 1–9 (2014).

31. Chiu, I. M. *et al.* Transcriptional profiling at whole population and single cell levels reveals somatosensory neuron molecular diversity. *Elife* **3,** 1–32 (2014).

32. Weiss, S. *et al.* Multipotent CNS stem cells are present in the adult mammalian spinal cord and ventricular neuroaxis. *J. Neurosci.* **16,** 7599–609 (1996).

33. Eagleson, K. L. & Bennett, M. R. Survival of purified motor neurones in vitro: Effects of skeletal muscle-conditioned medium. *Neurosci. Lett.* **38,** 187–192 (1983).

34. Goetz, J. J. & Trimarchi, J. M. Single-cell Profiling of Developing and Mature Retinal Neurons. *J. Vis. Exp.* **0,** 1–7 (2012).

35. Satija, R., Farrell, J. A., Gennert, D., Schier, A. F. & Regev, A. Spatial reconstruction of single-cell gene expression data. *Nat. Biotechnol.* **33,** 495–502 (2015).

36. Harrison, M. *et al.* Vertebral landmarks for the identification of spinal cord segments in the mouse. *Neuroimage* **68,** 22–29 (2013).

37. Shneider, N. A., Brown, M. N., Smith, C. A., Pickel, J. & Alvarez, F. J. Gamma motor neurons express distinct genetic markers at birth and require muscle spindle-derived GDNF for postnatal survival. *Neural Dev.* **4,** 42 (2009).

38. Friese, A. *et al.* Gamma and alpha motor neurons distinguished by expression of transcription factor Err3. *Proc. Natl. Acad. Sci. U. S. A.* **106,** 13588–93 (2009).

39. Johansson, H., Sjölander, P. & Sojka, P. Activity in receptor afferents from the anterior cruciate ligament evokes reflex effects on fusimotor neurones. *Neurosci. Res.* **8,** 54–59 (1990).

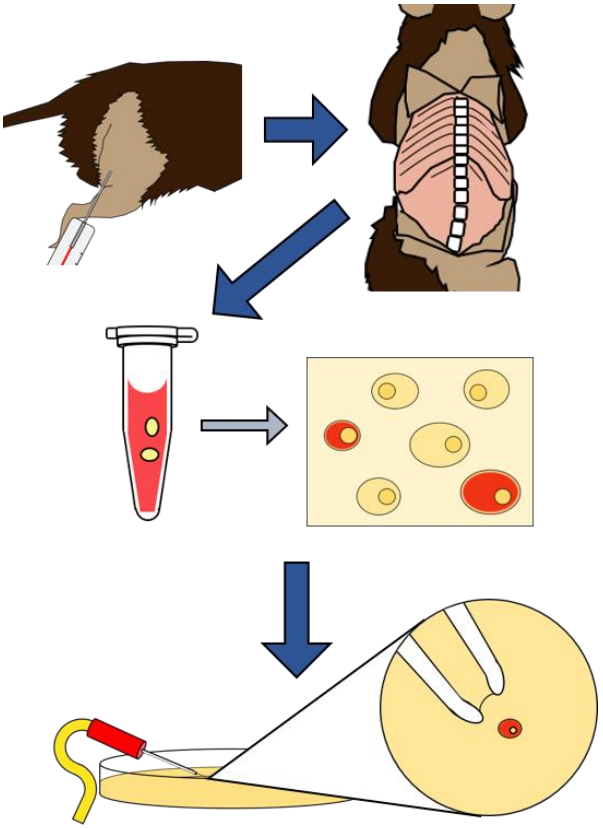

Figure 1. Flowchart for the protocol design

Animals are first injected in the biceps femoris (BF) muscle with DiI (top left). After allowing the dye to trace for at least 1 week, animals are sacrificed, and spinal tissue from the lumbar enlargement is collected, as well as DRG from L4 through L6 ipsilateral to the injection (top right). Collected and trimmed tissue is then dissociated through the appropriate protease enzyme to separate the cells (middle panel). Cells are then placed in a petri dish under a fluorescent microscope, where a glass micropipette can be used to collect individual cells that fluoresce red, and place them in lysis buffer (bottom panel).

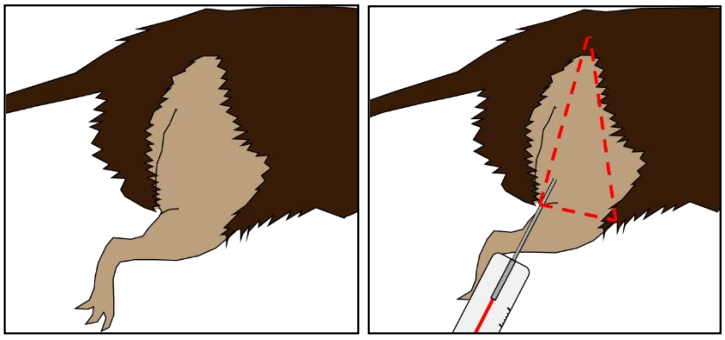

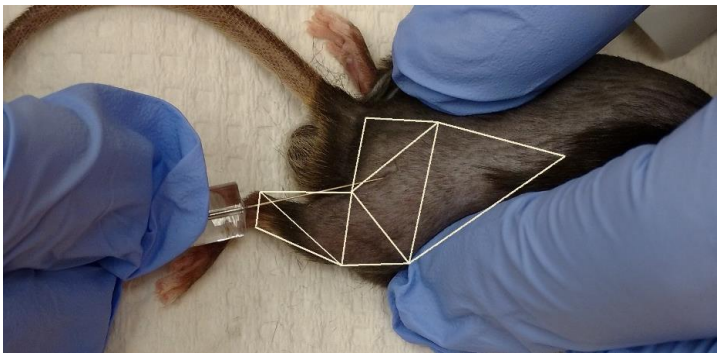

Figure 2. Injecting DiI into the biceps femoris.

Knowing anatomical landmarks can be helpful to ensure the proper muscle is injected. The biceps femoris can be located by drawing an imaginary triangle between the back of the knee, the front of the knee joint, and the hip joint. Injections posterior to this area are likely to accidentally label the semitendinosus.

Figure 3. Dissections for mouse neural tissue.

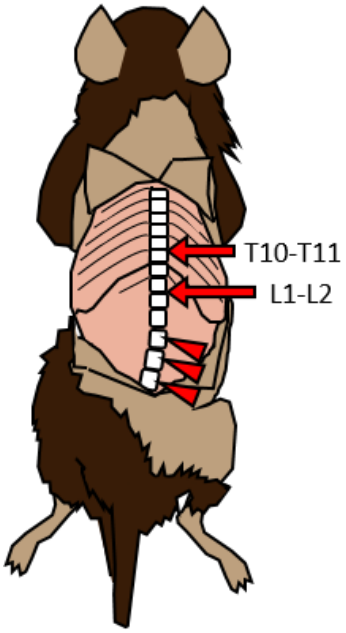

When the mouse has been euthanized, and its back is shaved and sprayed, make and incision along the midline and another across the skin of the back. Pull back the skin, and then use small scissors to remove the muscles from the spine. Locate the vertebrae junctions at T10-T11 and L1-L2 (arrows). The lumbar enlargement is typically located between these two points. These vertebrae are best located by finding the last floating rib, which marks the back of T13, and counting from there. Carefully remove the lamina of the spine by gently lifting with forceps while clipping the sides with spring scissors. Using a scalpel or razor blade, cut out the caudal half of the lumbar enlargement. DRG should be retrieved after spinal tissue. Cells traced from the biceps femoris should be found in L4-L6 (arrowheads). These can be found just inside the corresponding vertebrae, as small nodes on spinal nerves.

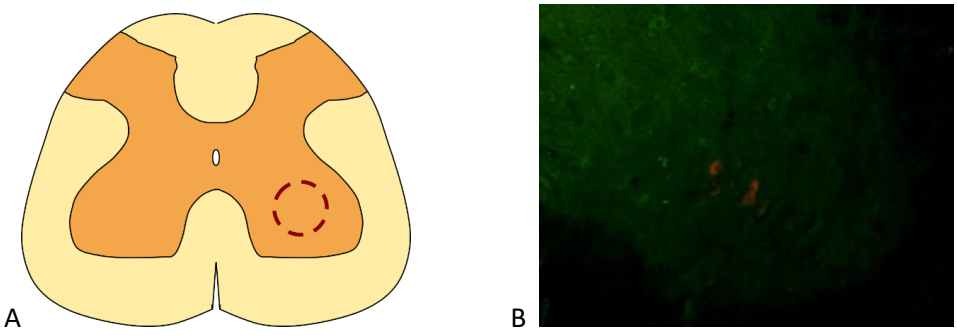

Figure 4. Traced neurons were observed in expected regions.

Previous studies have demonstrated that MNs innervating the hamstring are typically located in the internal portion of the ventral horn between L3 and L6 (A). 5 days after DiI injection, mice were euthanized, and SC samples from the lumbar enlargement (L2 to L6) were taken, perserved in PFA, and sectioned on a cryostat. Fluorescence microscopy (B) using green autofluorescence to delineate the white matter demonstrates that BF-traced cells were found in this area.

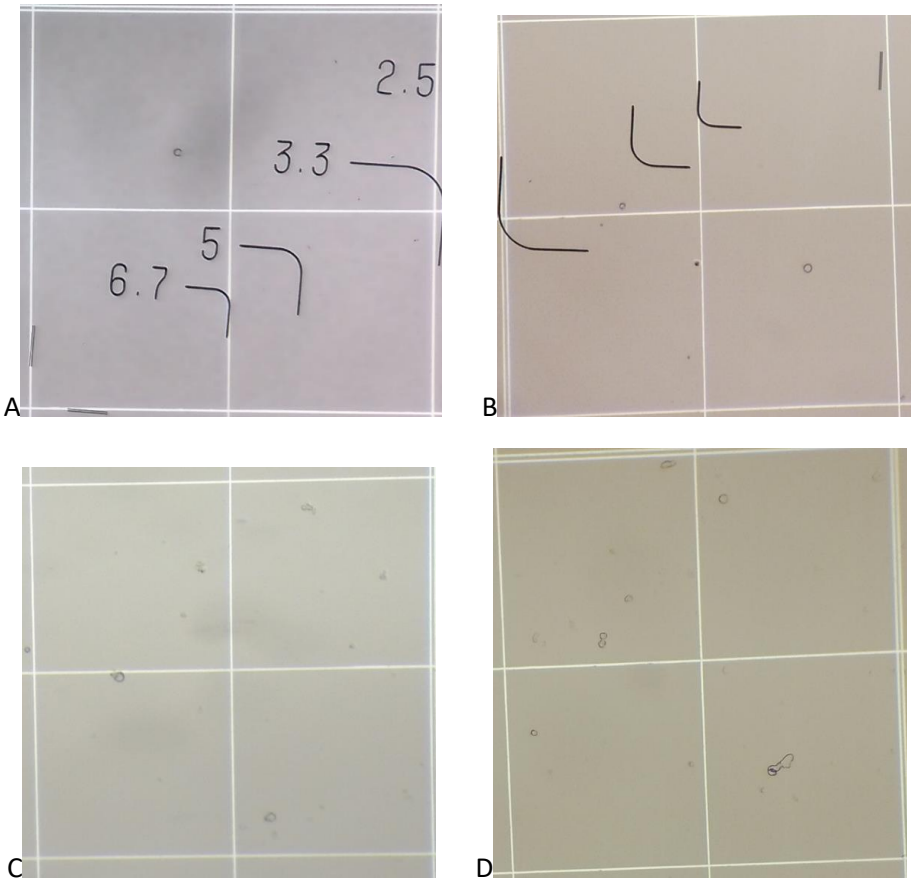

Figure 5. Assessment of dissociation techniques.

Different enzymatic dissociations were used to assess which had better output in each type of tissue. Cells were suspended in BSA and a sample was placed in a hemocytometer. JPEG images were taken through the 20× objective on an upright microscope. For each image, four 1mm×1mm squares were imaged. Using ImageJ, measurements were calibrated to the length of a segment within each square (250 µm) and each cell was traced and the area measured. For DRG samples, L5 and L6 from the right side in animals 1 and 3 were dissociated using papain followed by collagenase/dispase (A), while samples from 2 and 4 were dissociated using just the collagenase/dispase solution (B). From each animal, the VH from one side was dissociated using collagenase and dispase (C), whereas the other side was dissociated using collagenase alone (D). We did not see a sufficient number of cells large enough to be neurons in any of the samples. This is likely due to tissues having been stored frozen in RNA*later* for extended periods of time.

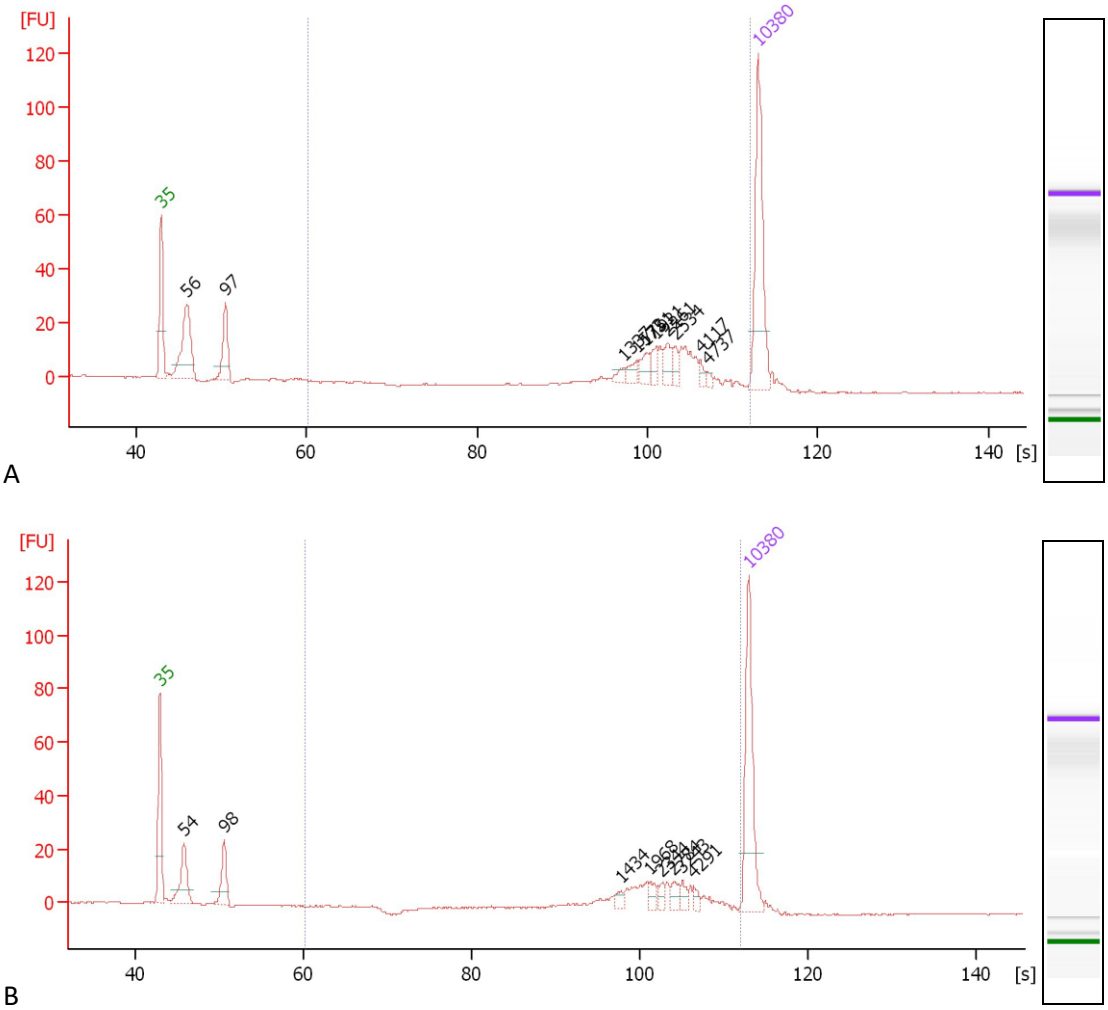

Figure 6. Quantification of cDNA from Single Cells

RNA samples from lysed single cells were reverse transcribed and amplified using kits from ClonTech. Quantity of cDNA was assessed on an Agilent Bioanalyzer. Fluorescence units (FU) are marked on the y-axis, while the x-axis marks the time in seconds. Quantity is determined via area-under-the-curve using upper and lower markers of known size and concentration as well as a ladder well. The bars on the left are virtual gel lanes derived from the respective data. (A) A smear analysis of a sample from 30 pg RNA positive control shows a yield of 1.67 ng cDNA (98.26 pg/µL, 17 µL). (B) A smear analysis from a sample of a single-cell lysate from the same experiment shows a yield of 1.49 ng cDNA (87.43 pg/µL, 17 µL).

CONCLUSIONS

Significance of Proprioceptive Deficits and Possible Mechanisms

Proprioception is an essential sensory modality for proper motor function and quality of life. Information is transmitted initially by large-diameter A-fibers innervating Golgi tendon organs (GTOs) and muscle spindles[1–3]. Muscle spindle sensitivity is mechanically modulated by input from γ-motoneurons (γ-MNs)[4,5], which in turn receive signaling from GTOs[6,7], thus completing a full synergistic circuit.

Disruption of proprioceptive input from the limbs is a common and poorly understood consequence of major injuries[8–14], often lasting beyond repair of the affected region of the body. A common cause for proprioceptive abnormalities is the rupture of the anterior cruciate ligament (ACL/CCL)[9,10,12,13,15–17]. Patients with ACL deficient knees have problems detecting knee motion and position[9,12], and feelings of "giving way" last in many patients even following successful reconstruction[14,18]. This feeling is likely associated with a change in the hamstring reflex which responds to ACL stretch[14,17,19–21]. A better understanding of this phenomenon could improve patient care, as proprioceptive function is linked to satisfaction and return to previous activity[14].

A model that may provide a blueprint for approaching this topic is the response of nociceptive neurons to injury and inflammation. Transient and long-term changes in the molecular phenotype of DRG nociceptors lead to hypersensitivity and mechanical allodynia[22,23]. This typically occurs through the interaction of neuroinflammation, calcium-mediated signaling, and changes to the membrane potential. Activity of proteins such as activating transcription factor 3 (ATF3) and p38 MAPK is increased in all cell types after injury in all cell types in the

DRG[23,24]. In nociceptors, these proteins have been shown to be important in either mediating or regulating inflammatory responses and increased sensitivity to stimuli[24–31]. It is possible that the increased activity of these proteins in proprioceptors activates similar pathways. While increased sensitivity and action potential rate in nociceptors has been tied to upregulation of TTX-resistant sodium channel activity[25,26], it is unknown whether a comparable event occurs in proprioceptors.

The similar changes in signal-cascade proteins between proprioceptors and nociceptors provides an opportunity for research into molecular mechanisms of proprioceptive pathology. This thesis proposes several methods for analyzing both primary proprioceptors and associated γ-MNs. The first technique was to section the CCL in a rodent model, and use a gene profiling array to assess changes in the lumbar DRG. Following this, a protocol was developed to retrogradely trace neurons of the hamstring muscles, pick out labeled cells from dissociated tissue, and procure cDNA libraries from single cells for gene expression analysis. Conclusions from these techniques are summarized below.

Changes Following CCL Rupture

No gene was significantly upregulated or downregulated in whole Lumbar DRG three weeks after knee surgery. This is likely due to the late timepoint, as many inflammatory neural responses occur within the first few days after injury [26,29,32–34]. This experiment also analyzed RNA from whole-DRG homogenates. Out of thousands of neurons and thousands more glial cells in a single ganglion, knee joint afferents comprise at most 300 cells in a lumbar DRG[35]. Future work in this field would benefit from more targeted approaches to the proprioceptors of the knee joint.

There were phenomena of note in the results of the arrays. The tendency toward upregulation of matrix metalloproteinase 9 (MMP-9) in DRGs ipsilateral to lesioned knees could be reflective of the after-effects of MMP-9 regulation occurring across the first week after surgery[29]. Furthermore, the expression of neurotrophin 4 (NTF4) was slightly but consistently upregulated in the lesioned side compared to the contralateral, but not was not upregulated in sham-operated animals. This could have implications in pain[36–38] or nerve recovery[39].

Further experiments into sensory neuron response to CCL-rupture, and indeed all such proprioceptive-response studies, should distinguish between the profiles of individual cells rather than relying on gross RNA collection. Also, the potential upregulations of MMP-9 and NTF4 reinforce the need to focus on analogs within proprioceptors to pain. In the next paper, a protocol is constructed to accomplish this by labeling cells based on target tissue, and isolating cells from within the target tissue.

Retrograde Tracing and Single-Cell Isolation

In the final chapter of this thesis, a protocol was developed to address the challenges of analyzing proprioceptive responses to injury on a cellular level. Retrograde tracing with the fluorescent dye DiI was used to identify neurons based on their target tissue. This was determined to be the optimal choice among tracing dyes due to its long detectable lifespan in living tissue[40]. The model was developed using the mouse biceps femoris (BF) as a model. This allows the tracing both sensory and motoneurons, providing for a more comprehensive look at proprioceptive circuitry. Additionally, tracing of motoneurons and sensory neurons from the BF is well characterized[41,42]. At the desired timepoint, spinal cord ventral horns and dorsal root ganglia were collected from the traced side and dissociated using a solution of collagenase and

dispase or papain followed by collagenase and dispase[43–45]. Single cells are then picked for RNA analysis[46,47].

During assessment of the phases of the protocol, histological sections of caudal lumbar spinal cord and DRG were both consistent with the findings of previous researchers[41,42]. Furthermore, cDNA synthesis and amplification with the SMART-Seq v4 kit from Clontech reliably produced the expected amount of cDNA from positive control RNA wells, and one cell collected from a rat in early practice of the technique also produced a testable amount of quality cDNA.

There were setbacks to the development of the protocol, and it was not carried out in its complete sequence. Most cells collected did not yield any cDNA. It is unclear, at this time, whether this is due to a failure single-cell collection technique or the RNA-extraction technique. Additionally, few cells large enough[48–51] to be sensory neurons or γ-MNs were found in any of the dissociated samples. This is likely because time constraints required the storage of samples at -80° C for up to a month before dissociation. In practice, neural tissue should be dissociated immediately after dissection.

Despite the setbacks, we have confidence in the feasibility of this protocol. Similar single-cell collection techniques for gene expression assays have been successful[46,47]. Indeed, the procedure for preparing the cells was derived from that of Setija and colleagues to prepare samples for RNA-Seq[47]. Additionally, using gene expression profiles, afferent cells can be sorted into cell type based on cell-type-specific markers. The same can be done for distinguishing γ-MNs from α-MNs[50,51]. Further applications of the technique could be applied to other muscles or joints of interest.

Integration and Further Implications

Though there no few positive results in our CCL-rupture experiment, there is still much potential for research on this topic. Our observation of MMP-9 upregulation in DRG after CCL lesion suggests that we achieved an inflammatory model in nociceptors[26,29]. Retrograde tracing has also been successfully used on joint afferents[35,40,52], so the protocol defined in Chapter III can be applied as well. The challenge faced that circumstance, however, would be the relatively low number of the dissociated neurons that would trace to the knee joint.

Further studies could also examine for effects damage on neurons that act synergistically with those of the damaged region. For instance, γ-MNs can be analyzed using the tracing and dissociation protocol. Hamstring proprioceptive afferents are sensitized in response to CCL stretch via synaptic connection between GTOs and γ-MNs[53]. A possible experiment to explore this would be to see if the altered pattern of input from the tendon afferents had a phenotypic effect on γ-MNs.

Overall, this information presents a promising frontier into the functioning of the peripheral nervous system. Further study into the molecular mechanisms of proprioceptive change and disruption could be a source of information for therapeutic paradigms. If a neuroinflammatory model underlies the persistent proprioceptive deficit in injury models, mediators of this response may become potential drug targets. In addition to this, a deeper understanding of the relationship between activity and the progression and outcome of inflammatory responses could better inform decisions in physical therapy.

References

1. Hunt, C. C. The effect of stretch receptors from muscle on the discharge of motorneurons. *J. Physiol.* **117,** 359–79 (1952).
2. Eccles, R. M. & Lundberg, A. Integrative pattern of Ia synaptic actions on motoneurones of hip and knee muscles. *J. Physiol.* **144,** 271–298 (1958).
3. Fukami, Y. Responses of isolated Golgi tendon organs of the cat to muscle contraction and electrical stimulation. *J. Physiol.* **318,** 429–443 (1981).
4. Kuffler, S. W., Hunt, C. C. & Quilliam, J. P. Function of medullated small-nerve fibers in mammalian ventral roots; efferent muscle spindle innervation. *J. Neurophysiol.* **14,** 29–54 (1951).
5. Bessou, P., Emonet-Denand, F. & Laporte, Y. Motor fibres innervating extrafusal and intrafusal muscle fibres in the cat. *J. Physiol.* **180,** 649–672 (1965).
6. Sjölander, P., Johansson, H., Sojka, P. & Rehnholm, a. Sensory nerve endings in the cat cruciate ligaments: a morphological investigation. *Neurosci. Lett.* **102,** 33–38 (1989).
7. Miyatsu, M. *et al.* The physiology of mechanoreceptors in the anterior cruciate ligament. *J. Bone Jt. Surg.* **75B,** 653–657 (1993).
8. Hankey, G. J. & Edis, R. H. The utility of testing tactile perception of direction of scratch as a sensitive clinical sign of posterior column dysfunction in spinal cord disorders. *J. Neurol. Neurosurg. Psychiatry* **52,** 395–398 (1989).
9. Barrett, D. S. Proprioception and function after anterior cruciate reconstruction. *J. Bone Jt. Surg.* **73,** 833–837 (1991).
10. Tyler, T. F., McHugh, M. P., Gleim, G. W. & Nicholas, S. J. Association of KT-1000

measurements with clinical tests of knee stability 1 year following anterior cruciate ligament reconstruction. *J. Orthop. Sports Phys. Ther.* **29,** 540–545 (1999).

11. Jerosch, J., Prymka, M. & Castro, W. H. M. Proprioception of the knee joints with a lesion of the medial meniscus. *Acta Orthop. Belg.* **62,** 41–45 (1996).
12. Reider, B. *et al.* Proprioception of the knee before and after anterior cruciate ligament reconstruction. *Arthroscopy* **19,** 2–12 (2003).
13. Katayama, M. *et al.* Proprioception and performance after anterior cruciate ligament rupture. *Int. Orthop.* **28,** 278–281 (2004).
14. Melnyk, M., Faist, M., Gothner, M., Claes, L. & Friemert, B. Changes in stretch reflex excitability are related to 'giving way' symptoms in patients with anterior cruciate ligament rupture. *J. Neurophysiol.* **97,** 474–480 (2007).
15. Beard, D. J., Kyberd, P. J., Fergusson, C. M. & Dodd, C. a. Proprioception after rupture of the anterior cruciate ligament. An objective indication of the need for surgery? *J. Bone Joint Surg. Br.* **75,** 311–315 (1993).
16. Courtney, C., Rine, R. M. & Kroll, P. Central somatosensory changes and altered muscle synergies in subjects with anterior cruciate ligament deficiency. *Gait Posture* **22,** 69–74 (2005).
17. Friemert, B. *et al.* Intraoperative direct mechanical stimulation of the anterior cruciate ligament elicits short- and medium-latency hamstring reflexes. *J. Neurophysiol.* **94,** 3996–4001 (2005).
18. Krogsgaard, M. R., Fischer-Rasmussen, T. & Dyhre-Poulsen, P. Absence of sensory function in the reconstructed anterior cruciate ligament. *J. Electromyogr. Kinesiol.* **21,**

82–86 (2011).

19. Dyhre-Poulsen, P. & Krogsgaard, M. R. Muscular reflexes elicited by electrical stimulation of the anterior cruciate ligament in humans. *J. Appl. Physiol.* **89,** 2191–2195 (2000).

20. Tsuda, E., Okamura, Y., Otsuka, H., Komatsu, T. & Tokuya, S. Direct evidence of the anterior cruciate ligament-hamstring reflex arc in humans. *Am. J. Sports Med.* **29,** 83–87 (2001).

21. Schoene, M. *et al.* The reliability of a method for measuring the anterior cruciate ligament-hamstring reflex: An objective assessment of functional knee instability. *Knee Surgery, Sport. Traumatol. Arthrosc.* **17,** 1107–1116 (2009).

22. Jin, S.-X., Zhuang, Z.-Y., Woolf, C. J. & Ji, R.-R. p38 Mitogen-Activated Protein Kinase Is Activated After a Spinal Nerve Ligation in Spinal Cord Microglia and Dorsal Root Ganglion Neurons and Contributes To the Generation of Neuropathic Pain. *J. Neurosci.* **23,** 4017–4022 (2003).

23. Ji, R. R., Samad, T. A., Jin, S. X., Schmoll, R. & Woolf, C. J. p38 MAPK activation by NGF in primary sensory neurons after inflammation increases TRPV1 levels and maintains heat hyperalgesia. *Neuron* **36,** 57–68 (2002).

24. Tsujino, H. *et al.* Activating transcription factor 3 (ATF3) induction by axotomy in sensory and motoneurons: A novel neuronal marker of nerve injury. *Mol. Cell. Neurosci.* **15,** 170–182 (2000).

25. Yan, C., Wang, H. & Boyd, D. D. ATF3 represses 72-kDa type IV collagenase (MMP-2) expression by antagonizing p53-dependent trans-activation of the collagenase promoter. *J. Biol. Chem.* **277,** 10804–10812 (2002).

26. Holvoet, S., Vincent, C., Schmitt, D. & Serres, M. The inhibition of MAPK pathway is correlated with down-regulation of MMP-9 secretion induced by TNF-?? in human keratinocytes. *Exp. Cell Res.* **290,** 108–119 (2003).

27. Shortland, P. J. *et al.* ATF3 expression in L4 dorsal root ganglion neurons after L5 spinal nerve transection. *Eur. J. Neurosci.* **23,** 365–373 (2006).

28. Chattapadhyay, S., Myers, R. R., Janes, J. & Shubayev, V. Cytokine regulatino of MMP-9 in peripheral glia: implications for pathological processes and pain in injured nerve. *Brain. Behav. Immun.* **21,** 561–568 (2007).

29. Nascimento, G. C., Rizzi, E. & Gerlach, R. F. Expression of MMP-2 and MMP-9 in the rat trigeminal ganglion during the development of temporomandibular joint inflammation. *Braz. J. Med. Biol. Res.* **46,** 956–967 (2013).

30. Su, J. *et al.* Phenotypic changes in dorsal root ganglion and spinal cord in the collagen antibody-induced arthritis mouse model. *J. Comp. Neurol.* **523,** 1505–1528 (2015).

31. Rau, K. K. *et al.* Cutaneous tissue damage induces long-lasting nociceptive sensitization and regulation of cellular stress- and nerve injury-associated genes in sensory neurons. *Exp. Neurol.* **283,** 413–427 (2016).

32. Bulling, D. G., Kelly, D., Bond, S., McQueen, D. S. & Seckl, J. R. Adjuvant-induced joint inflammation causes very rapid transcription of beta-preprotachykinin and alpha-CGRP genes in innervating sensory ganglia. *J. Neurochem.* **77,** 372–82 (2001).

33. Seino, D. *et al.* The role of ERK signaling and the P2X receptor on mechanical pain evoked by movement of inflamed knee joint. *Pain* **123,** 193–203 (2006).

34. Wu, Q. & Henry, J. L. Functional changes in muscle afferent neurones in an osteoarthritis

model: Implications for impaired proprioceptive performance. *PLoS One* **7,** 1–10 (2012).

35. Salo, P. T. & Theriault, E. Number, distribution and neuropeptide content of rat knee joint afferents. *J. Anat.* **190 (Pt 4,** 515–522 (1997).

36. Fan, G. *et al.* Knocking the NT4 gene into the BDNF locus rescues BDNF deficient mice and reveals distinct NT4 and BDNF activities. *Nat. Neurosci.* **3,** 350–7 (2000).

37. Zhou, L. J. *et al.* Limited BDNF contributes to the failure of injury to skin afferents to produce a neuropathic pain condition. *Pain* **148,** 148–157 (2010).

38. Ichikawa, H. *et al.* Masseteric nerve injury increases expression of brain-derived neurotrophic factor in microglia within the rat mesencephalic trigeminal tract nucleus. *Cell. Mol. Neurobiol.* **31,** 551–559 (2011).

39. English, A. W., Cucoranu, D., Mulligan, A., Rodriguez, J. a & Sabatier, M. J. Neurotrophin-4/5 is implicated in the enhancement of axon regeneration produced by treadmill training following peripheral nerve injury. *Eur. J. Neurosci.* **33,** 2265–2271 (2011).

40. Choi, D., Li, D. & Raisman, G. Fluorescent retrograde neuronal tracers that label the rat facial nucleus: A comparison of Fast Blue, Fluoro-ruby, Fluoro-emerald, Fluoro-Gold and DiI. *J. Neurosci. Methods* **117,** 167–172 (2002).

41. Bácskai, T., Rusznák, Z., Paxinos, G. & Watson, C. Musculotopic organization of the motor neurons supplying the mouse hindlimb muscles: A quantitative study using Fluoro-Gold retrograde tracing. *Brain Struct. Funct.* **219,** 303–321 (2014).

42. Mohan, R., Tosolini, A. P. & Morris, R. Targeting the motor end plates in the mouse hindlimb gives access to a greater number of spinal cord motor neurons: An approach to maximize retrograde transport. *Neuroscience* **274,** 318–330 (2014).

43. Malin, S. a, Davis, B. M. & Molliver, D. C. Production of dissociated sensory neuron cultures and considerations for their use in studying neuronal function and plasticity. *Nat. Protoc.* **2,** 152–160 (2007).

44. Bosmans, F., Puopolo, M., Martin-Eauclaire, M.-F., Bean, B. P. & Swartz, K. J. Functional properties and toxin pharmacology of a dorsal root ganglion sodium channel viewed through its voltage sensors. *J. Gen. Physiol.* **138,** 59–72 (2011).

45. Thériault, O. & Chahine, M. Correlation of the electrophysiological profiles and sodium channel transcripts of individual rat dorsal root ganglia neurons. *Front. Cell. Neurosci.* **8,** 1–9 (2014).

46. Goetz, J. J. & Trimarchi, J. M. Single-cell Profiling of Developing and Mature Retinal Neurons. *J. Vis. Exp.* **0,** 1–7 (2012).

47. Satija, R., Farrell, J. A., Gennert, D., Schier, A. F. & Regev, A. Spatial reconstruction of single-cell gene expression data. *Nat. Biotechnol.* **33,** 495–502 (2015).

48. Moqrich, A. *et al.* Expressing TrkC from the TrkA locus causes a subset of dorsal root ganglia neurons to switch fate. *Nat. Neurosci* **7,** 812–818 (2004).

49. Chen, C., Zhou, X. F. & Rush, R. A. Neurotrophin-3 and trkC-immunoreactive neurons in rat dorsal root ganglia correlate by distribution and morphology. *Neurochem.Res.* **21,** 809–814 (1996).

50. Shneider, N. A., Brown, M. N., Smith, C. A., Pickel, J. & Alvarez, F. J. Gamma motor neurons express distinct genetic markers at birth and require muscle spindle-derived GDNF for postnatal survival. *Neural Dev.* **4,** 42 (2009).

51. Friese, A. *et al.* Gamma and alpha motor neurons distinguished by expression of

transcription factor Err3. *Proc. Natl. Acad. Sci. U. S. A.* **106,** 13588–93 (2009).

52. Hanesch, U. & Heppelmann, B. A simple method for a specific retrograde labelling of dorsal root and sympathetic ganglion cells innervating the knee joint of the cat. *J. Neurosci. Methods* **63,** 55–59 (1995).

53. Johansson, H., Sjölander, P. & Sojka, P. Activity in receptor afferents from the anterior cruciate ligament evokes reflex effects on fusimotor neurones. *Neurosci. Res.* **8,** 54–59 (1990).